

Controlled electrochemical growth and magnetic properties of CoFe2O4 nanowires with high internal magnetic field

Nabil Labchir, Abdelkrim Hannour, Abderrahim Ait Hssi, Didier Vincent, Patrick Ganster, Ahmed Ihlal

▶ **To cite this version:**

Nabil Labchir, Abdelkrim Hannour, Abderrahim Ait Hssi, Didier Vincent, Patrick Ganster, et al.. Controlled electrochemical growth and magnetic properties of CoFe2O4 nanowires with high internal magnetic field. Journal of Alloys and Compounds, 2021, 868, pp.159196. 10.1016/j.jallcom.2021.159196 . ujm-03268956

HAL Id: ujm-03268956
https://ujm.hal.science/ujm-03268956

Submitted on 10 Mar 2023

HAL is a multi-disciplinary open access archive for the deposit and dissemination of scientific research documents, whether they are published or not. The documents may come from teaching and research institutions in France or abroad, or from public or private research centers.

L'archive ouverte pluridisciplinaire **HAL**, est destinée au dépôt et à la diffusion de documents scientifiques de niveau recherche, publiés ou non, émanant des établissements d'enseignement et de recherche français ou étrangers, des laboratoires publics ou privés.



Distributed under a Creative Commons Attribution - NonCommercial 4.0 International License

Version of Record: https://www.sciencedirect.com/science/article/pii/S0925838821006046
Manuscript_cef5b3bf1d5f4d70080e8d9b1b29a9cc

Controlled electrochemical growth and magnetic properties of $CoFe_2O_4$ nanowires with high internal magnetic field

Nabil Labchir[1,2*], Abdelkrim Hannour[2], Abderrahim Ait Hssi[2] , Didier Vincent[1], Patrick Ganster[3], Ahmed Ihlal[2]

[1]Univ Lyon, UJM-Saint-Etienne, CNRS, LabHC, UMR 5516, F-4203, Saint-Étienne, France

[2]Univ Ibn Zohr, Faculty of Sciences Agadir, LabMER, BP 8106, Cité Dakhla, 80000, Agadir, Morocco

[3]Ecole de Mines de Saint-Étienne, Centre SMS, Laboratoire Georges Friedel CNRS-UMR5307, F-42023 Saint-Étienne, France

* Corresponding author: nabil.labchir@univ-st-etienne.fr

Abstract

Self-polarized ferrimagnetic nanowires of $CoFe_2O_4$ are electrochemically grown by the electrodeposition technique in AAO membranes. XRD, EDS and SQUID analysis confirm the formation of highly stoichiometric $CoFe_2O_4$ nanowires with high magnetic response into 20 nm -AAO membrane. SEM and AFM images revealed a total filling of the AAO membrane with Co and Fe at an applied potential of -1.2 V. In addition, the electrodeposition and cooling in the presence of an applied magnetic field improve the magnetic response of $CoFe_2O_4$ nanowires. The SQUID measurements confirmed the elaboration of $CoFe_2O_4$ nanowires with an internal magnetic field of 1.52 T. As a result, this ferrimagnetic nanowired substrate will be suitable for future miniaturized self-biased microwave devices.

Keywords: Cobalt ferrite, Self-polarized ferrimagnetic nanowires, AAO membranes, electrodeposition, magnetic properties, microwave devices.

1. Introduction

In recent years, the field of nanomaterials and nanotechnology has emerged as one of the most attractive areas for scientists in both fundamental and technological terms due to the wide range of possible applications [1]. The ferrimagnetic nanowires have been included in this category. They have potential applications in various fields, including the development of self-biased miniaturized devices. Cobalt ferrite ($CoFe_2O_4$) is a ferrimagnetic material widely recognized and

© 2021 published by Elsevier. This manuscript is made available under the CC BY NC user license
https://creativecommons.org/licenses/by-nc/4.0/

employed in many applications due to its high coercivity, high saturation magnetization and strong magnetic anisotropy. $CoFe_2O_4$ nanowires are widely used for magnetoresistive sensors, magnetic random access memories, microwave devices [2,3]. For this reason, in the past, several papers dealing with the structure and magnetic properties of $CoFe_2O_4$ nanowires, elaborated by different methods, have been published [4-6]. It has been highlighted that the magnetic behavior of $CoFe_2O_4$ depends on the structure which is related to the method and conditions of elaboration. However, more detailed investigations on $CoFe_2O_4$ nanowires have been carried out due to the evolution of the elaboration techniques as well as the characterization techniques [7-9]. Recently, scientists have focused on the study of $CoFe_2O_4$ deposited in nanoporrous membranes, with the objective of studying the magnetic behavior of this material in these porous templates. The bibliographical study, carried out in our work, has attracted our attention to the recent work performed on the deposition of $CoFe_2O_4$ nanowires. Unfortunately, there is very limited studies on the enhancement of the magnetic properties of $CoFe_2O_4$ nanowires with a very detailed approach. From there, we wished to focus our research on the development of a low cost, fast and easy technique to elaborate a hard ferrimagnetic $CoFe_2O_4$ nanowires. The chemical synthesis techniques have made such progress that it is now possible to develop magnetic nano-objects of complex shapes, especially nanowires with a defined shape. This specific shape gives the objects notable magnetic properties [10,11]. Among the chemical methods for synthesizing nanostructures, we have used the electrodeposition under magnetic field (magneto-electrodeposition) as a technique to synthetize $CoFe_2O_4$ nanowires. In the present paper, we will focus on the magneto-electrodeposition of $CoFe_2O_4$ nanowires in AAO nanoporous membranes. The effects of the experimental parameters such as AAO pore diameter, applied potential, magnetic field and annealing temperature on the electrochemical, structural, morphological, elementary composition and magnetic properties will be discussed.

2. Experimental

Commercially available Anodic aluminium oxide (AAO) membranes (Anodisc 13, Whatman, UK) with a variable average pore diameter ranging from 20 to 200 nm, a nominal thickness of 60 µm and pores density of 10^9 pores/cm^2 (50% porosity), were used as supports of the electrochemical growth of nanowires. These AAO membranes were coated via rf sputtering by a thin layer of cupper to serve as the working electrode as shown in **Fig.1**.

Fig.1 (Here)

The platinum sheet served as counter electrode and an Ag/AgCl electrode was used as reference electrode. All the electrodes are connected to a three electrode setup, controlled by a potentiostat (PGZ 301, Voltamaster 4), allowing the electrodeposition of Co and Fe into AAO membranes (see Figure 2). The distance between the working electrode and the counter electrode in all experiments was 1.5 cm. All the electrodes have the same exposed surface to the electrolyte. In order to find the right electrochemical synthesis protocol for $CoFe_2O_4$, several concentrations and pH values were systematically tested at room temperature (25 °C). The working concentrations adopted for a 100 mL of an electrolyte are 0.06 M of $FeSO_4$, 0.04 M of $CoSO_4$, 0.12 M of (NH4)2SO4, 0.08 M of H2SO4 and 0.4 M of H_3BO_3. All chemical products have analytical purity (99%, Sigma Aldrich) and have been used as received. During the cathodic reaction, the evolution of hydrogen can lead to the precipitation of hydroxides (if the pH is not maintained constant at the solution-electrode interface). To avoid this harmful phenomenon for the quality of the deposit, the bath pH is adjusted to 3 by H_2SO_4 and stabilized by the addition of the boric acid (H_3BO_3), which compensates for the loss of protons since it decomposes according to the reaction:

$$H_3BO_3 + H_2O \rightarrow H_2BO_3^- + H_3O^+ \quad (1)$$

Its action being, according to the literature, highest at about pH of 4 and is very commonly used as a buffering agent in electrodeposition baths [12]. Before starting the electroplating process, the AAO membranes were ultrasonically cleaned for 10 minutes with acetone and double distilled water. Three NdFeB permanent magnets (30 mm diameter and 15 mm height), have been separately placed for each growth test under the AAO membrane. These magnets produce a static magnetic field ranging from 0.4 to 0.6 T perpendicular to the working electrode. In the electrochemical growth of $CoFe_2O_4$ composite, the applied potential was ranged from -1 to -1.2 V versus Ag/AgCl at room temperature.

Fig.2 (Here)

Characterization: The XRD spectra of $CoFe_2O_4$ nanowires was recorded using X'Pert PRO X-ray diffractometer (λ_{Cu} = 1.5406 Å) in the angular range 15-82° with a step size of 0.03° at room temperature. The XRD data are processed by FullProf program. Then, the morphology and the elementary composition of the nanowires have been examined by scanning electron microscope (SEM-Quanta 200-FEI) operating at 20 kV and equipped with energy-dispersive X-ray detector. Moreover, the hysteresis loops of the ferrimagnetic

$CoFe_2O_4$ nanowires have been measured by a superconducting quantum interface device magnetometer (MPMS SQUID VSM)

3. Results and discussion

3.1 Cyclic Voltametric study

The cyclic voltammetry (CV) is an electrochemical technique used in order to evaluate the suitable potentials region of metals growth. The CV curve of the precursor solution was directly performed on the AAO membranes. The potential sweep was ranged from 0 to -1.3 V with a scan rate of 30 mV/s. Therefore, for simultaneous co-deposition of Co and Fe metals, the deposition potential should be such the deposition potential of individual metals, comes closer to each other. It is known that the standard reduction potentials at room temperature for the Fe and Co metals are -0.44 V and -0.28 V, respectively [13].

Fig.3 (Here)

According to **Fig. 3**, the oxidation peak of CoFe composite is appeared at -0.28 V. The singular peaks of Co^{2+} and Fe^{2+} reduction are masked by the water reduction, which is kinetically more favorable on aqueous bath. Moreover, the voltammogram shows an increase of the cathodic current with negative scan of the electrode potential from -0.9 to -1.2 V, which might be related to the reduction of Co and Fe ions as described by the following equations:

$$Co^{2+} + 2e^- \rightarrow Co \quad (2)$$

$$Fe^{2+} + 2e^- \rightarrow Fe \quad (3)$$

From -1.2 down to -1.3 V, the current density increases rapidly, showing another reaction except for the reduction of ions. Indeed, in the case of an applied potential more than -1.2 V, a large bubbles appeared on the AAO membrane surface which can significantly affect the electrochemical growth of CoFe composite. As a matter of fact, in order to grown electrochemically the CoFe composite without the generation of hydrogen bubbles, it is recommended to apply a potential less than -1.3 V.

3.2 Effects of the pore diameter of the AAO membrane

Chronoamperometry study

The chronoamperometry analysis provides information of the nucleation and growth mechanisms. Especially, the synthesis duration and the critical overflow time of the deposit from the pores. **Figure 4** shows the chronoamperograms recorded during the growth of CoFe composite within the AAO membranes of different nominal diameters (20 nm, 100 nm, 200 nm).

Fig.4 (Here)

The synthesis conditions are the same for every sample, i.e. an applied potential of -1.2 V and an identical membrane exposed surface of 1 *cm* in diameter. As shown in **Fig.4**, in the early stages of the electrochemical growth, the establishment of the diffusion layer contributes to the decrease of the current density. Once the diffusion layer is occurred, the growth of the wires takes place inside the porous AAO membrane. The current density is quasi-static during the pore filling (zone 1), then the pores become completely filled (zone 2). In addition, hemispherical overflow caps are starting to be formed (zone 3) on the outer face of the AAO membrane, which increases the deposition area and thus, the current density. Finally, in the last phase (zone 4), the current density continues to rise when the entire upper surface of the membrane is covered and a thin film is growing as shown in **Fig.5**. Similar behaviors have been reported by Riveros et al. [14].

Fig.5 (Here)

Moreover, we noticed that the current density of the electrochemical reduction of Co and Fe ions during the phase 1 is more important as the pore diameter increases. Indeed a very close current density values of -0.74 mA, -0.80 mA, and -0.85 mA for the AAO membranes with 20, 100, and 200 nm in diameter pore have been observed, respectively. This small difference in the resulting current density is explained by the difference in the electrochemically active surface of the working electrode, which can be related to the geometry defects of the wires after the copper metallization. Moreover, we can see that the synthesis time that is required to fill the AAO membrane pores is almost the same, i.e. around 40 min.

Structural and morphological properties

Figure 6.b shows the X-ray diffractograms of the samples electrodeposited electrodeposited at -1.2 V into various nanoporous AAO membranes and annealed at 500 ^{o}Cfor 24 hours.

Fig. 6 (Here)

The formation of the spinel phase of $CoFe_2O_4$ within the AAO membranes was confirmed by the appearance of these characteristic peaks in the XRD patterns (*JCPDS* n^o. 22−1086). The obtained spectra for the synthesized $CoFe_2O_4$ nanowires indicate that the samples are well crystallized and polycrystalline. Moreover, the analyses revealed the birth of three other peaks located at $2\theta = 37.11^o$, $2\theta = 71.5^o$ and $2\theta = 79.8^o$, which are assigned respectively to the plans (222), (620) and (444). In addition, the XRD spectra revealed the presence of a strong diffraction intensity of the plane (331) for all elaborated samples, indicating the presence of a partial orientation along this reflection. The AAO membrane peaks were designated by Al_2O_3. The crystallographic lattice parameter a of the spinel phase of $CoFe_2O_4$ crystallized in face-centred cubic (fcc), was determined for the higher peak (331) in all XRD spectra using the following equation:

$$\mathrm{a} = \frac{\lambda\sqrt{h^2 + k^2 + l^2}}{2\ sin(\theta)} \tag{4}$$

The calculated values are 8.378 Å, 8.382 Å and 8.386 Å for the $CoFe_2O_4$ embedded in AAO membranes of 200, 100 and 20 nm in pore diameter, respectively. The calculated value for a is in good agreement with the standard lattice constant value reported in the literature [15].

Williamson and Hall proposed that the total enlargement of XRD peaks is originated from the sum of the enlargement due to the size and to the defects, with the simplifying assumption that all the contributions have a lorentzian character; so, they established the following equation [16]:

$$\beta_{hkl}\ \cos\theta = \frac{0.9\lambda}{D} + 4\varepsilon \sin\theta \tag{5}$$

The instrumental broadening β_{hkl} is corrected from the adjustment of the XRD peaks by using the following equation:

$$\beta_{hkl} = \sqrt{(\beta_{hkl})^2_{Measured} - (\beta_{hkl})^2_{Standard}} \tag{6}$$

The best approach to make this correction and to determine the standard broadening is to anneal the sample at high-temperature. The elaborated samples are annealed at 850 ^oC for 24 hours. This heat treatment will remove not only the stored strain energy, but also the broadening associated to small crystallites. As a result, a deposit consisting of large

crystallites can be obtained. Then, the Williamson-Hall standard formula is used to extract the corrected values of β_{hkl} from the sample without large crystallites.

Therefore, **Eq.5** is a straight-line equation. Accordingly, the Williamson-Hall plot consists of plotting the points on a graph, with known coordinates, on a graph. A linear regression and Y-Intercept extrapolation of the experimental points allow to obtain the parameters of the line and deduce the value of the crystallite size D and the slope ε.

$$D = \frac{0.9\lambda}{Y_{Intercept}} \tag{7}$$

$$\varepsilon = slope \tag{8}$$

This protocol has been adopted for all the synthesized samples in this work.

Figure 6.a shows the XRD spectrum of the annealed sample at 850 ^{o}C. It can be noticed that the peaks become very fine which indicates the formation of large crystallites inside the AAO membrane pores. The crystallite size of $CoFe_2O_4$ nanowires was evaluated from the XRD line broadening using the Williamson-Hall method.

The calculations revealed that the $CoFe_2O_4$ nanowires grown into AAO membranes of 200 and 100 nm in pore diameter have approximately 40.25 and 32.21 nm in crystallite size, respectively. However, the sample grown into AAO membrane of 20 nm in pore diameter has 14.05 nm in crystallite size.

Moreover, the morphology of the nanowires embedded into AAO membranes with different pore sizes has been studied using SEM microscopy. To do this, all membranes are firstly immersed for a duration of 30 s in a diluted iron perchloride solution for removing the copper serving as cathode. Next, the samples are then dissolved in 1 M of sodium hydroxide (NaOH) for 40 min in order to remove the alumina from the elaborated nanocomposites. This protocol is illustrated in **Fig.7**.

Fig.7 (Here)

Fig.8 (Here)

As shown in **Fig. 8.a**, **b** and **c**, the top view images revealed that the electrodeposited $CoFe_2O_4$ nanowires are completely filled and have average diameters of 200, 100 and 20 nm, respectively. These values are approximately equal to the pore diameters of the AAO templates. The cross-sectional images of the nanowires are shown in **Fig. 8.d**, **e** and **f**. They show that the nanowires are well filled and oriented after the dissolution process.

On the other hand, the chemical composition was examined in various zones of the samples in order to study the effect of the pore diameter variation on the stoichiometry of the electrodeposited nanowires (**Table. 1**).

Table 1 (Here)

The EDS spectra indicate the existence of peaks corresponding to Co, Fe and O. The Al peaks originate from the residues of the alumina membranes. In addition, no copper peak is detected, confirming that 30 s of sample immersion in the iron perchloride solution is sufficient to completely remove the copper film. Indeed, the purity of the synthesized samples could be confirmed by the absence of any impurities in the EDS spectra. From the table.1, it can be concluded that the average atomic ratios of O, Co and Fe vary from (62.25%, 12.81% and 22.72%) to (58.08%, 14.2% and 26.41%) as the pore diameter decreasing from 200 to 20 nm. This enhancement could be justified by the fact that the decreasing pore diameter promotes the formation of a pure $CoFe_2O_4$ spinel phase. As a result, the nanowires deposited in AAO membranes of 20 nm in pore diameter possess a high stoichiometry of O, Co and Fe elements.

Magnetic properties

The magnetic properties of the developed nanowires have been measured using a SQUID magnetometer. The electrochemical synthesis was interrupted before the deposition over-flow from the pores of AAO membranes to avoid any kind of thin layer on the surface of the nanowires. During the measurement, the magnetic field was systematically applied parallel to the nanowires. **Figure 9** shows the hysteresis cycles measured at 300 K for $CoFe_2O_4$ nanowires with different pore diameters of AAO membranes (200, 100, and 20 nm).

Fig. 9 (Here)

Table.2 summarizes the estimated magnetic parameters characterizing the $CoFe_2O_4$ nanowire arrays.

Table 2 (Here)

The measurements reveal that the nanowires array is ferrimagnetic. Moreover, it is noted that the squareness ratio (M_r/M_s) and the coercive field (H_c) increase as the diameter of the nanowires decreases (pore diameter) from 200 to 20 nm. This enhancement is generally attributed to the transition from a dominated mode with magnetic domains in large diameter nanowires (200 nm) towards a monodomain mode in small diameter nanowires. The critical diamater (D_c) that produced the monodomain structure of $CoFe_2O_4$ is estimated using the following formula [17]:

$$D_c = \frac{9}{2\pi M_s^2}\sqrt{\frac{2k_bT_cK_1}{\mathrm{a}}} \qquad (9)$$

where $K_1 = 2.5\ 10^5\ erg/cm^3$ is the magnetocrystalline anisotropy constant, $T_c = 800\ K$ the Curie temperature, k_b the Boltzmann constant, and a the lattice parameter. For $D > D_c$, the particles exist in a multidomain structure, while for $D > D_c$, the particles exist in a monodomain structure.

The estimated value of D_c is about 14.47 nm, which is comparable to the average diameter (14.05 nm) of the synthesized $CoFe_2O_4$ crystallite. So the grown $CoFe_2O_4$ crystallites into the pores of 20-nm-diameter show rather a monodomain behavior. This result indicates the dominance of the shape anisotropy for the nanowires inside the pores of 20-nm-diameter. Furthermore, the EDS measurements (**Table.1**) emphasized that the chemical stoichiometry of the spinel structure is better for the nanowires of 20 nm. In this case, the reduction of the crystallite size confirmed by the XRD analyses can be considered as an additional reason to explain the modification of the magnetic properties. The obtained results are in good agreement with previous literature reports [18,19]. Therefore, we decided to only work with the membrane in 20 nm of pore diameter due to the best magnetic response.

3.3 *Effects of the applied potential*

Chronoamperometry study

Figure 10 presents the CA curves obtained during the deposition of the CoFe composite into AAO membranes of 20 nm in the pore diameter, at several applied potentials.

Fig.10 (Here)

From the recorded CA curves, at the early stages of the electrochemical reduction a non-faradaic process is involved resulting from the double layer charging (DLC) in which Co and Fe ions migrate to the bottom of the AAO membrane pores [20]. Then, a new phase of stable current, reflecting the growth of CoFe in the nanopores, appears. Moreover, the current density was clearly increased in absolute value with the rising of the applied deposition potential, which justifies the difference and the delay in the starting increase of the current density for the potentials -1.1 V and -1 V. In addition, the CA results indicate that the pore filling time tends towards 55 and 70 min for the applied potentials -1.1 V and -1 V, respectively. On the other hand, a duration of 40 min is sufficient for a total pore filling in the case of -1.2 V, which corroborates the enhanced nucleation efficiency of the CoFe composite. The observations of the pore-filling time drop is in accordance with Faraday's law ($Q = i\ t$), which suggests that more the reduction current of ions increases more the pore filling time is reduced. In this context, a good reproducibility is achieved in the different electrodeposition experiments. After this first deposition step, all the electrodeposited samples were annealed at 500 ^{o}C in air for 24 hours in order to promote the formation of the $CoFe_2O_4$ spinel phase and also to keep the AAO membranes more thermally stable.

Structural and morphological properties

The crystalline structure of the nanowires electrodeposited at various potentials was explored by XRD as shown in **Fig. 6.c**.

Table 3 (Here)

The recorded XRD spectra suggest that all the elaborated nanowires possess a spinel phase, confirming the growth of $CoFe_2O_4$ into the porous AAO membranes according to the JCPDS standard data (n^{o}. 22−1086). Moreover, the XRD patterns revealed that the all nanowires exhibited a partial orientation along the (311) reflection. However, we can note the appearance of a new peak of $CoFe_2O_4$ at $2\theta = 79.8^{o}$ for the nanowires deposited at -1.1 V. Furthermore, for the nanowires electrodeposited at -1.2 V, the XRD spectra emphasized the birth of two new peaks at $2\theta = 71.62^{o}$ and $2\theta = 37.36^{o}$ corresponding to spinel $CoFe_2O_4$ phase. The lattice parameters were determined for the intense reflection (311) of each spectrum. As a consequence,

the lattice parameter (a) was found to be 8.325 Å, 8.331 Å and 8.354 Å for the nanowires electrodeposited at -1 V, -1.1 V and -1.2 V, respectively. Indeed, the obtained values are in good agreement with that corresponding to $CoFe_2O_4$ single-crystals (a = 8.394 Å). The average crystallite size (D) for $CoFe_2O_4$ sample is also calculated from XRD data using the Williamson-Hall method. The calculations revealed that the crystallite size of the $CoFe_2O_4$ depends on the applied potential. In fact, the average crystallite size decreases from 15.17 to 14.04 nm for the applied potentials of -1 V and -1.2 V, respectively. Moreover, the XRD investigations globally indicate that the crystallinity degree is enhanced as the applied voltage becomes more negative. The evolution of the lattice parameter and crystallite size is associated to the fact that the crystallites agglomerations become smaller by varying the applied potential from -1 V to -1.2 V. Within this context, similar results are reported recently by Franco et al. [21].

Figure 11 shows the SEM images that evaluated the effect of the potential variation on the morphology and the ratio of the pore-filling. The electrodeposition time was interrupted at 40 min in order to evaluate the difference in the pore-filling of the AAO membranes.

Fig.11 (Here)

As shown in **Fig.11**, the filling ratio of the AAO membrane pores strongly depends on the applied voltage. **Figure.11.c** reveals that a total and uniform pore-filling with $CoFe_2O_4$ crystallites is reached at -1.2 V for 40 min, unlike the samples deposited at -1 and -1.1 V, contain unfilled pores as observed in **Fig.11.a** and **b**. In this case, the samples need more time to reach the total filling of the pores as indicated in the CA curves (**Fig.10**). This difference in the pore filling ratio arises from various phenomena that have occurred during the electrochemical growth of metal ions in the AAO membrane. However, the thickness reduction of the diffusion layer, that controls the dynamic of ions, can drastically affects the kinetics of the diffused ions from the electrolyte to the pores, thus modifying the nucleation and the growth rate. Consequently, the structure and the composition of the $CoFe_2O_4$ nanowires showed a noticeable modification. The diameter of the elaborated nanowires is ranging from 20 to 23 nm, which is roughly equal the pore diameter of the used AAO membrane. In addition, the elementary composition of the synthesized nanowires, investigated by the EDS analysis (**Table. 4**), confirms that no relevant impurities are detected inside the $CoFe_2O_4$ nanowires. Moreover, the EDS analysis revealed a better stoichiometry of the $CoFe_2O_4$ nanowires with 16.44%- Co, 25.81%-Fe and 57.92%-O obtained with an applied potential of -1.2 V.

Table 4 (Here)

This result indicates the good arrangement of the Co, Fe, O cations in the tetrahedral and octahedral sites of the elementary lattice of $CoFe_2O_4$ and confirms the good formation of the spinel phase for the $CoFe_2O_4$ nanowires. As a matter of fact, the obtained stoichiometry degree confirms again the birth of the new peaks observed in the XRD spectrum for a pure spinel phase.

As shown in **Fig.12**, the AFM probing technique was used to characterize the topography of $CoFe_2O_4$ nanowires elaborated by electrodeposition at various applied potentials.

Fig.12 (Here)

As a preliminary step, the 3D AFM images are recorded in tapping mode in order to determine the surface topography of the different samples. AFM images of the $CoFe_2O_4$ nanowires deposited at -1 V and -1.1 V clearly confirm the absence of the total pore-filling. The surface of both samples is generally rough and contains many areas with different levels and lengths of nanowires. In addition, the surface of the nanowires deposited at -1.2 V shows a total pore filling. The surface is very homogeneous and compact, which confirms that the pores are completely filled by the $CoFe_2O_4$ crystal. The AFM results greatly reproduced the SEM observations discussed in the previous paragraph

Magnetic properties

The magnetic properties of the $CoFe_2O_4$ nanowire arrays grown at different deposition potentials have been measured at room temperature under an applied field up to 1500 kA/m. **Fig. 13** displays the variation of squareness ratio M_r/M_s as a function of the applied field H.

Fig.13 (Here)

Their corresponding magnetic parameters are listed in Table 5

Table 5 (Here)

We have investigated the evolution of the magnetic properties of $CoFe_2O_4$ nanowire arrays as a function of their average chemical composition. Thus, within the elementary composition ranges between 28.39% and 16.44% of Co as shown in EDS spectra (**Table. 4**) for the applied potential varying from -1 V to -1.2 V, it was found that the nanowires grown at -1.2 V exhibit a quasi-perfect stoichiometry. Table 5 reveals that the squareness ratio and coercive field are enhanced in both parallel and perpendicular directions as the applied field negatively increases. Therefore, the nanowires deposited at -1.2 V present high squareness ratio of 0.41 and coercivity H_c of 118 kA/m along the wire axis, in comparison to squareness ratio of 0.36 and coercivity of 111 kA/m in the perpendicular direction. It is obvious that the squareness ratio and the coercivity are highly affected by the elementary composition of $CoFe_2O_4$ into AAO membrane. The magnetic response of the $CoFe_2O_4$ nanowires is closely related to the cations distribution in tetrahedral and octahedral sites of spinel phase and also the crystallographic microstructure [22]. Due to the rapid growth of Co and Fe metals into AAO membrane pores with the variation of the applied potentials from -1 V to -1.2 V, the intrinsic stress and defects increase with the decrease of Co atoms in the nanopores. As a consequence, this enhances the crystallographic structure to obtain a pure spinel phase. From the recorded hysteresis loops, it has been observed that at -1.2 V, the easy axis is slightly controlled by the shape anisotropy of $CoFe_2O_4$ crystallites into the nanopores. Indeed, there is a remarkable improvement in the coercivity parallel and perpendicular to the wire axis when the applied voltage is maintained at -1.2 V. Indeed, this effect is expected due to the decrease in the crystallite size as shown in XRD analysis (i.e. transition from multidomain state to monodomain one), as well as the more efficiency reduction of Fe^{2+} and Co^{2+} metallic ions. It has been reported that the crystallites deposited at -1 and -1.1 V possess comparable sizes (15.17 nm, 14.76 nm) with the monodomain size (14.47 nm). On the other hand, the crystallite deposited at -1.2 V has a size of 14.04 nm, so the formation of the monodomain state can be ensured. Within this context, similar findings have been reported by Wu et al. [23]. Moreover, the internal magnetic field (H_i) acting inside the $CoFe_2O_4$ nanowires embedded into AAO template, can be expressed in the remanent state by the following formula [24]:

$$H_i = H_a - NM_s \tag{10}$$

where H_a is the anisotropy field of $CoFe_2O_4$ nanowires, and N is the demagnetizing factor, close to 0 in the case of an elongated magnetic cylinder polarized vertically along the z axis. The H_a value is experimentally determined by the intersection between the edges of the

hysteresis cycles in the both measurement directions as described in **Fig.13**. Table 5 summarizes the values collected for H_a. As expected, the nanowires electrochemically grown at -1.2 V exhibit an anisotropy field of 1.4 T. In this case, the internal magnetic field H_i of the $CoFe_2O_4$ nanowires is proportional to the anisotropy field, and we can approximatively write $H_i \cong H_a$

The results reached in this section are encouraged to maintain -1.2 V as a reduction potential for Co and Fe ions in the future electrodeposition experiments of this work.

3.4 *Effects of applied magnetic field*

Chronoamperometry study

To investigate the effect of the magnetic field on the electrochemical growth of Co and Fe within AAO membranes, chronoamperometric curves have been recorded during the electrodeposition process (**Fig.14**). The CoFe nanowires were electrodeposited at room temperature in potentiostatic mode (deposition potential fixed at -1.2 V).

Fig.14 (Here)

.

As displayed in **Fig.14**, the resulting current density of CoFe reduction into AAO membranes increases when the applied magnetic field B ranges from 0.4 to 0.6 T. However, the current density enhancement is mainly explained by the fact that the migration of the electro-active species towards the bottom of the nanopores becomes faster in the presence of the magnetic field B which decreases the thickness of the DLC according to the following formula [25]:

$$\delta_D = 1.59\left(\rho R \nu^{1/3} D^{1/3}\right)^{1/3} (nFC)^{-1/3} B^{-1/3} \qquad (11)$$

where R is the radius of the working electrode, ρ the density of electrolyte, ν the bulk flow velocity, n the electron number, F the Faraday constant, D the diffusion coefficient, and C the concentration of electroactive ions in the electrolyte.

Indeed, in the case of the system with mass transport control, the limiting current density of diffusion increases with B and the species concentration gradient ΔC following the law [26]:

$$j = 0.45 R \pi^{-1} \gamma (nFD)^2 (V/D)^{2/3} (\nu\eta)^{-1} \Delta C^2 B \qquad (12)$$

where γ is the rotation efficiency introduced by the deviation from the ideal parallel arrangement of current lines, and η the dynamic viscosity.

Thus, the amount deposited increased with the D.C applied magnetic field. As a result, the total filling time of AAO membrane nanopores is reduced from 37 to 30 min as displayed in **Fig.14**, which confirms our results. During the electrochemical analysis for the electrochemical growth of CoNiMo films, Aaboubi et al. [27] have reported that the presence of the magnetic field modifies the polarization curves and clearly increases the current density of growth. Such result is obtained in our work, indicating the presence of the MHD convection responsible for enhancing the rate of ions transferred to the active deposition surface. This process is illustrated in **Fig.15**.

Fig.15 (Here)

From the adopted scheme, two types of MHD convections are produced by the action of Lorentz force: (i) a macroscopic MHD convection around the AAO membrane edges, and (ii) a micro-MHD convection around the nonequilibrium fluctuations such as hemispherical diffusion zones around each pore.

Structural and morphological properties

In order to determine the effect of the applied magnetic field on the $CoFe_2O_4$ microstructure, the X-ray diffraction technique was employed. **Figure 6.d** shows three diffractograms obtained for the magneto-electrodeposited nanowires at -1.2 V with B = 0.4 T, 0.5 T and 0.6 T, after annealing for 24 hours at 500 ^oC.

From these diffractograms, the formation of the spinel phase of cobalt ferrite is confirmed by the presence of these characteristic peaks. Moreover, the XRD spectra show that the magnetic field partially increases the enlargement and intensities for the different peaks with a partial texture following the crystallographic direction [311]. The shown result reveals that the $CoFe_2O_4$ nanowires exhibit a higher degree of crystallinity. Quantitatively, the lattice parameter (a) and the average crystallite size (D) have been evaluated by exploiting the XRD data. The calculations have revealed that the magneto-electrodeposition decreases the crystallite size into the nanopores from 12.82 to 10.54 nm, and also shifted the lattice parameter from 8.361 Å to 8.383 Å, which approaches to the value of bulk cobalt ferrite (8.394 Å). In conclusion, the growth is strongly affected by the action of the magnetic field. This effect is attributed to the micro-MHD convection acting on the ions during the cathodic

reaction. The bias magnetic field controls and enhances the current density (**Fig.14**), thus promoting a constant growth of the germs. This would explain the modifications of the $CoFe_2O_4$ crystalline properties such as texture and structure [28]. The observed XRD results are in good agreement with those reported by Ganesh et al. [29].

Moreover, the morphologies of the magneto-electrodeposited $CoFe_2O_4$ were examined using SEM analysis after the samples dissolution in 1 M of NaOH for 40 min. **Figure 16** presents the nanowires deposited for various filling times (30, 35 and 37 min), corresponding to each value of the applied magnetic field as described in **Fig.14**.

Fig.16 (Here)

As observed in the top SEM images, the pores of the AAO membranes are well filled by the $CoFe_2O_4$ crystal. The diameter of the nanowires is ranging from 20 to 22 nm, which is nearly equivalent to the nominal diameter of the used AAO membranes. The elementary composition of $CoFe_2O_4$ nanowires was investigated by the EDS analysis (**Table. 6**). As indicated by the collected data in the tables, the nanocomposite consisted only of Fe, Co and O, which confirms its purity. Moreover, it was observed that the nanocomposite magneto-electrochemically grown at 0.6 T presents a great stoichiometry (15.15% - Co, 28.54% -Fe and 56.31% –O). In addition, this stoichiometry confirms the higher crystallinity of $CoFe_2O_4$ and the formation of the spinel phase with regular distribution of Co and Fe ions on the tetrahedral and octahedral sites. Moreover, this result can explain the increasing of XRD reflections enlargements and intensities shown in **Fig. 6.d**. It is quite conceivable that for the ferromagnetic ions, the induced magnetic dipolar effects can have significant influence on the crystallographic distribution within the spinel structure of $CoFe_2O_4$ [30].

The AFM technique was used to investigate the surface uniformity. **Figure 17** shows the AFM 2D surface topography of the $CoFe_2O_4$ nanowires deposited at different applied magnetic fields.

Fig.17 (Here)

The samples have uniform and well-filled nanopores, especially for the sample deposited at 0.6 T, as shown by SEM analysis. Basically, under the effect of the applied magnetic field

increase, the movement of ions in the electrolyte, the mass transport speed towards the electrochemically active surface and the MHD convection generated from Lorentz force reach their maximum levels. This is reflected by a remarkable enhancement of the current reduction (**Eq.12**), which corresponding to the formation of deposit inside the AAO pores. As a result, the surface of the deposit becomes more compact and homogeneous as the magnetic field increases **Fig. 17.a, b** and **c**.

Magnetic properties

The normalized M–H curves of $CoFe_2O_4$ nanowires magneto-electrochemically grown in the AAO membranes are obtained at 300 K for an applied scanning field parallel and perpendicular to the wire axis. **Figure 18** shows the hysteresis loops of the annealed samples.

Fig.18 (Here)

Table 7 summarizes the estimated magnetic parameters characterizing the $CoFe_2O_4$ nanowire arrays.

Table 7 (Here)

The measurements reveal that the application of the magnetic field modifies the magnetic properties by enhancing the squareness ratio, the coercive field, and the anisotropy field in both scanning directions (**Table 7**). They report a remarkable shifting from 0.47, 120 kA/m and 1.4 T to 0.55, 130 kA/m and 1.5 T for M_r/M_s, H_c and H_a of the magneto-electrodeposited nanowires at 0.4 and 0.6 T, respectively.

From an electrochemical and microstructural point of view, this phenomenon can be related to the mechanism of the reduction of Fe and Co ions, and also to the process of growth during the electrodeposition. The electrochemical growth in the magnetic field is influenced by an additional convection and the crystallites growth is favorable in the direction of the easiest magnetization. The nucleation rate is increased and small crystallites can uniformly grow since the convection near the interface provides sufficient magnetic ions to each crystallite. In this case, the reduction of the crystallite size in the presence of the magnetic field is essentially due to the increase of the nucleation rate, as confirmed by the XRD analysis, and can be considered as a key point to tailoring the magnetic properties of the cobalt ferrite nanocomposite. Furthermore, the EDS measurements emphasize that the chemical

composition of nanowires is enriched in cobalt as the applied magnetic field increases from 0.4 T to 0.6 T, which eventually forms a highly pure spinel phase inside the nanopores. These results could be explained by uniaxial magnetic anisotropy and the appearance of the single magnetic domain structure, i.e. induced by the walls displacement of the local domains formed between the clusters of crystallites, leading to a partial orientation on the magnetic moments into the AAO membranes. Moreover, its shape anisotropy favors the alignment of the easy axis along the nanowires. Consequently, these mentioned factors enhance the internal magnetic field H_i that greatly depends on the anisotropy field H_{a} estimated from the measured hysteresis loops. The current results of the magnetic measurements of our samples have shown a great similarity with those previously reported [31-33].

In conclusion, we have demonstrated a significant improvement in the magnetic properties of the $CoFe_2O_4$ nanowires by applying an external magnetic field during the growth of the nanowires in 20 nm-AAO porous templates.

3. 5 *Effects of the annealing on the magnetic properties*

Figure 19 presents the room-temperature hysteresis curves for the magneto-electrodeposited $CoFe_2O_4$ nanowires at 0.6 T/-1.2 V and annealed at two different temperatures.

Fig. 19 (Here)

The experimental data of the hysteresis loops i.e. squareness ratio M_r/M_s, coercive field H_c and anisotropy field H_{a} are displayed in Table 8.

Table 8 (Here).

Accordingly, there is a significant difference in the magnetic response of the annealed nanowires. The nanowires corresponding to the annealing temperature (600 ^oC) have a M_r/M_s of 0.52, H_c of 73 kA/m and 1.12 T for H_{a}. On the other hand, the nanowires annealed at 700 ^oC possess a M_r/M_s of 0.43, 60 kA/m for H_c and 1.01 T for H_{a}. In principle, the magnetic properties are highly sensitive to the crystallite size, microstructures and distributions of cations into tetrahedral and octahedral sites in the spinel structure [34]. The cations distribution is influenced by various parameters such as the ionic radius of the cations, the stabilization energy in the crystalline field, the electronic configuration, etc. The

distribution of the individual cations in the unit cell can be described by the following chemical formula:

$$(Co_{1-i}^{2+}Fe_{i}^{3+})[Co_{i}^{2+}Fe_{2-i}^{3+}] \quad (13)$$

where i is the degree of inversion. The ideal inverse spinel structures have $i = 1$ and $i = 0$ for the normal spinel and the mixed spinel structures, with the value of i varying between 0 and 1. The ions within square brackets are located in the octahedral sites and the ions within brackets are located in the tetrahedral sites.

In this context, the shown decrease of M_r/M_s with the increase of the annealing temperature can be attributed to the cations redistribution where Co^{2+} ions migrate from tetrahedral to octahedral sites and Fe^{3+} cations migrate from octahedral to tetrahedral sites with the increase of temperature from 600 ^oC to 700 ^oC. These phenomena will be responsible for a change in the degree of inversion i (**Eq. 13**) and therefore the formation of structural distortions due to structural disorder. This structural disorder will be accompanied by a magnetic disorder due to a non-alignment of the spins with the global magnetization direction of the crystal.

Accordingly, the net magnetic moment will be affected. The preference of the net magnetic moment of $CoFe_2O_4$ crystallites with the spinel structure is presented as [35]: $\boldsymbol{m} = \sum \boldsymbol{m_{octahedral}} - \boldsymbol{m_{tetrahedral}}$. It should be noted that the magnetic moment of Fe^{3+} ions is greater than that of Co^{2+} ions. As a matter of fact, the redistribution of Fe^{3+} ions at octahedral sites will increase the total number of the magnetic moment which appears as the decrease of M_r/M_s in the $CoFe_2O_4$ nanowires in parallel and perpendicular orientations.

Moreover, the reduction in coercivity and anisotropy field as the annealing temperature shifting from 600 ^oC to 700 ^oC can be associated with the increase in $CoFe_2O_4$ crystallite size inside the AAO membrane pores and the drop in the anisotropy constant of the samples. This weakening was corroborated by the finding that the XRD peaks become very fine and have small FWHM (β_{hkl}) (**Fig. 6.a**), which indicates such shape modification of the produced nanocrystallite, i.e. the transition from single separated nanocrystallite to compact nanocrystallite granules. These results are in agreement with those reported by Ajroudi et al. [36].

As a conclusion, the optimal temperature that provides the best magnetic properties for $CoFe_2O_4$ nanocomposite is around of 500 ^oC. This annealing temperature will be kept in the next examinations.

3. 6 *Magnetic Field cooling effects*

In this study, a lower rate cooling under magnetic field was performed in order to investigate its effect on the structural and magnetic properties of $CoFe_2O_4$ nanowires. The sample is magneto-electrodeposited at -1.2 V/0.6 T and then annealed for 24 hours at 500 ^oC. After this first step of synthesis, the sample was cooled under uniform static magnetic field (0.6 T) by placing it on the upper side of a permanent magnet, which is the same used during the electrochemical deposition, as shown in **Fig. 20.**

Fig.20 (Here)

Figure 6.e illustrates the XRD patterns of the elaborated $CoFe_2O_4$ nanowires. The XRD reflections correspond to cobalt ferrite (spinel structure). It can be noted that the cooling under magnetic field induces a new XRD reflection (422) of $CoFe_2O_4$ at $2\theta = 53.7^o$, which indicates the possible effect of the field cooling on the internal microstructure of nanowires. The calculated lattice parameter has a value of 8.387 Å. In addition, the Williamson-Hall calculation provides a crystallite size of 9.06 nm, which is smaller than those reported in the previously discussed studies of our work.

Figure 21 presents SEM observations of field cooled nanowires at 0.6 T after their dissolution in NaOH solution.

Fig. 21 (Here)

The images confirm that the AAO membrane pores are completely filled by the $CoFe_2O_4$ crystallites, as well as the presence of high density of nanowires.

In order to investigate the influence of the field cooling effect on the magnetic response of $CoFe_2O_4$ nanowires, hysteresis loops were measured at room temperature in the parallel and perpendicular orientations.

Fig. 22 (Here)

During the magnetic field cooling, the nano-crystallites were aligned in the direction of the magnetic field. From the performed curves, the easy axis is parallel to the nanowire axis and the perpendicular direction represents the hard axis. An interesting result was observed in the

hysteresis loops when the nanocrystals are aligned along the easy axis. This configuration promotes the spin order of the $CoFe_2O_4$ nano-crystallites, which increases the coercivity and remanent magnetization of the nanowire arrays. The increase in coercivity H_c (141 kA/m) and squareness ratio M_r/M_s (0.6) is attributed to the magnetocrystalline and shape anisotropies induced by the imposition of the magnetic field during the cooling process. Along the easy axis, the $CoFe_2O_4$ nanowires exhibit a large magnetic anisotropy due to magnetocrystalline anisotropy superimposed on the shape one. Moreover, the uniformity of nanowire lengths, reflected by the total filling of the AAO membrane pores, is a key parameter in the magnetic inversion process. A closely distributed nanowire lengths can lead to a coherent magnetization reversal process and result in enhanced coercivity and squareness of the loops. Generally, when the nanowires are aligned in the direction of the magnetic field, all the spins of the $CoFe_2O_4$ nano-crystallites are parallel to the easy axis. Thus, aligned nanowires may exhibit a partially square hysteresis loops. As a matter of fact, the higher M_r/M_s and H_c ratio might be attributed to two possible reasons: (i) the sizes of all nano-crystallites are smaller, i.e. single-domain regime, and (ii) magnetization curve are governed by coherent rotation of magnetic moments. As a result, partially auto-polarized ferrimagnetic $CoFe_2O_4$ nanowires that present magnetic response of hard material with an internal magnetic field of 1.52 T were obtained.

4. Conclusion

In summary, we have studied the physico-chemical properties of $CoFe_2O_4$ nano-crystallites embedded electrochemically in AAO membranes with different pore diameters (20, 100 and 200 nm) by different techniques (CV, CA, XRD, SEM-EDS, AFM, SQUID-VSM). As a first study, we have chosen to study the effect of pore diameters and the potential applied to the working electrode on the formation of $CoFe_2O_4$ deposit have been under consideration. The results show that the 20 nm-nanowires in diameter exhibit the best magnetic response. Then, we investigated the effect of the magnetic field presence during the electrochemical process. The magnetic field affects the nucleation and the electrochemical growth by changing the filling time of the AAO membrane pores. On the other hand, the convective effect of the magnetic field influences the morphology of $CoFe_2O_4$ deposits, where the crystallite size decreases, resulting in a change in the texture of the deposit. The magnetic characterizations of $CoFe_2O_4$ nanowires have shown that the magnetic field leads to a significant enhancement of the squareness ratio and coercive field of the synthesized nanowires. Moreover, the magnetic measurements have revealed that the cooling under magnetic field produces a better self-polarized magnetic composite with an

internal field of 1.52 T. Finally, the reached magnetic response of the $CoFe_2O_4$ nanowires can make them suitable for the auto-polarized microwave devices.

Declaration of interests

The authors declare that they have no known competing financial interests or personal relationships that could have appeared to influence the work reported in this paper.

Acknowledgments

The authors acknowledge the financial support of PHC-Toubkal under the project TBK/85/17, Campus France: 38983UH.

References

[1] V. Pokropivny, R. Lohmus, I. Hussainova, A. Pokropivny, S. Vlassov, Introduction to nanomaterials and nanotechnology, Tartu University, 2007

[2] N. Labchir, A. Hannour, A. A. Hssi, D. Vincent, J. P. Chatelon, D. Dufeu, M. Sajieddine, Microwave response of coplanar waveguide based on electrodeposited $CoFe_2O_4$ nanowires, J. Magn. Magn. Mater. 510 (2020) 166952. https://doi.org /10. 1016/ j.jmmm. 2020. 166952.

[3] C. H. Kim, Y. Myung, Y. J. Cho, H. S. Kim, S. H. Park, J. Park, B. Kim, Electronic structure of vertically aligned Mn-doped $CoFe_2O_4$ nanowires and their application as humidity sensors and photodetectors, J. Phys. Chem. **C.** 113 (2009) 7085-7090. https://doi.org/10.1021/jp900165c.

[4] G. Ji, S. Tang, B. Xu, B. Gu, Y. Du, Synthesis of $CoFe_2O_4$ nanowire arrays by sol–gel template method, Chem. Phys. Lett. 379 (2003) 484-489. https://doi.org/10.1016/ j.cple tt.2003.08.090.

[5] Y. W. Ju, J. H. Park, H. R. Jung, S. J. Cho, W. J. Lee, Fabrication and characterization of cobalt ferrite ($CoFe_2O_4$) nanofibers by electrospinning, Mater. Sci. Eng. **B**. 147 (2008) 7-12. https://doi.org/10.1016/j.mseb.2007.10.018.

[6] N. S. Gajbhiye, S. Srivastava, S. Kurian, B. R. Behta, V. N. Singh, Magnetic field assisted hydrothermal synthesis of $CoFe_2O_4$ nanowires, J. Phys. Conf. Ser. 200 (2010) 072093. https://doi.org/10.1088/1742-6596/200/7/072093.

[7] H. D. Chen, J. K. Xu, J. Q. Wei, P. F. Wang, Y. B. Han, J. C. Xu, J. Li, Mesoporous $CoFe_2O_4$ nanowires: Nanocasting synthesis, magnetic separation and enhanced catalytic degradation for ciprofloxacin, Phys. Chem. Solids. 132 (2019) 138-144. https://doi .o rg / 10.1016/j.jpcs.2019.04.008.

[8] H. Zheng, M. G. Han, L. J. Deng, 2016. Fabrication of $CoFe_2O_4$ ferrite nanowire arrays in porous silicon template and their local magnetic properties, Chinese. Physics. B. 25, 026201. https://doi.org/10.1088/1674-1056/25/2/026201.

[9] C. Pham-Huu, N. Keller, C. Estournes, G. Ehret, J. M. Greneche, M. J. Ledoux, Microstructural investigation and magnetic properties of CoFe2O4 nanowires synthesized inside carbon nanotubes, Phys. Chem. Chem. Phys. 5 (2003) 3716-3723. https:// doi.Org /10.1039/B304773C.

[10] N. Labchir, A. Hannour, D. Vincent, A. A. Hssi, M. Ouafi, K. Abouabassi, M. Sajieddine, Tailoring the Optical Bandgap of Pulse Electrodeposited $CoFe_2O_4$ Thin Films, J. Electron. Mater. 49 (2020) 2242-2248. https://doi.org/10.1007/s11664-019-07923-y.

[11] A. Ait Hssi, L. Atourki, N. Labchir, M. Ouafi, K. Abouabassi, A. Elfanaoui, K. Bouabid, Optical and dielectric properties of electrochemically deposited p-Cu_2O films, Mater. Res. Express. 7 (2020) 016424. https://doi.org/10.1088/2053-1591/ab6772.

[12] J. S. Santos, R. Matos, F. Trivinho-Strixino, E. C. Pereira, Effect of temperature on Co electrodeposition in the presence of boric acid, Electroch. Acta. 53 (2007) 644-649. https://doi.org/10.1016/j.electacta.2007.07.025.

[13] M. F. Ashby, D. R. H. Jones, Engineering Materials 1: An Introduction to Properties, Applications and Design, fourth ed., Elsevier, 2012.

[14] G. Riveros, H. Gómez, A. Cortes, R. E Marotti, E. A. Dalchiele, Crystallographically oriented single-crystalline copper nanowire arrays electrochemically grown into nanoporous anodic alumina templates, Appl. Phys. A. 81 (2005) 17-24. https://doi.org/10.1007/s00339-004-3112-1.

[15] N. Labchir, A. Hannour, A. A. Hssi, D. Vincent, K. Abouabassi, A. Ihlal, M. Sajieddine, Synthesis and characterization of $CoFe_2O_4$ thin films for solar absorber application, Mater. Sci. Semicond. Process. 111 (2020) 104992. https://doi.org/10.1016/j.mssp.2020.104992.

[16] G. Williamson, W. Hall, X-Ray Line Broadening from Filed Aluminium and Wolfram, Acta. Metall. 1 (1953) 22-31. https://doi.org/10.1016/0001-6160(53)90006-6.

[17] Z. Zi, Y. Sun, X. Zhu, Z. Yang, J. Dai, W. Song, Synthesis and magnetic properties of $CoFe_2O_4$ ferrite nanoparticles, J. Magn. Magn. Mater. 321 (2009) 1251-1255. https:/ /doi. org/10.1016/j.jmmm.2008.11.004.

[18] Z. L. Lu, P. Z. Gao, R. X Ma, J. Xu, Z. H. Wang, E. V. Rebrov, Structural, magnetic and thermal properties of one-dimensional $CoFe_2O_4$ microtubes, J. Alloys Compd. 665 (2016) 428-434. https://doi.org/10.1016/j.jallcom.2015.12.262

[19] R. Zhang, L.Sun, Z.Wang, W. Hao, E. Cao, Y. Zhang, Dielectric and magnetic properties of $CoFe_2O_4$ prepared by sol-gel auto-combustion method, Mater. Res. Bull. 98 (2018) 133-138.

[20] M.S. Kilic, M.Z. Bazant, A. Ajdari, Steric effects in the dynamics of electrolytes at large applied voltages I. Double-layer charging, Phys. Rev. E. 75 (2007) 021502. https://doi.org/10.1103/PhysRevE.75.021502.

[21] A. Franco, F.L.A. Machado, V.S. Zapf, Magnetic properties of nanoparticles of cobalt ferrite at high magnetic field, J. Appl. Phys. 110 (2011) 053913. https://doi org /10.1063 /1.3626931.

[22] C. H. Chia, S. Zakaria, M. Yusoff, S. C. Goh, C. Y. Haw, S. Ahmadi, H. N. Lim, Size and crystallinity-dependent magnetic properties of $CoFe_2O_4$ nanocrystals, Ceram. Int. 36 (2010) 605-609. https://doi.org/10.1016/j.ceramint.2009.10.001.

[23] Z. Wu, P. Niu, B. Yang, R. Yu, Effect of aspect ratio on microstructure and magnetic properties of spinel $CoFe_2O_4$ nanowire arrays, Appl. Phys. A. 105 (2011) 177. https://doi. org/10.1016/j.ceramint.2009.10.001.

[24] V. Laur, G. Vérissimo, P. Quéffélec, L.A. Farhat, H. Alaaeddine, E. Laroche, J.P. Ganne, Self-biased Y-junction circulators using lanthanum-and cobalt-substituted strontium hexaferrites, IEEE. Trans. Microw. Theory. Tech. 63 (2015) 4376–4381. https://doi.org /10.1109/TMTT.2015.2495218.

[25] M. Zieliński, E. Miękoś, Influence of constant magnetic field on the electrodeposition of Co–Mo–W alloys, J. Appl. Electrochem. 38 (2008) 1771. https://doi.org/10.1007/s10800-008-9628-x.

[26] A. Sugiyama, M. Hashiride, R. Morimoto, Y. Nagai, R. Aogaki, Application of vertical micro-disk MHD electrode to the analysis of heterogeneous magneto-convection, Electrochim. Acta. 49 (2004) 5115-5124. https://doi.org/10.1016/j.electacta.2004.06.024.

[27] O. Aaboubi, A. Y. Ali-Omar, A. Franczak, K. Msellak, Investigation of the electrodeposition kinetics of Ni–Mo alloys in the presence of magnetic feld, J. Electroanal. Chem. 737 (2015) 226–234. https://doi.org/10.1016/j.jelechem.2014.10.014.

[28] K. L. Rabah, J. P. Chopart, H. Schloerb, S. Saulnier, O. Aaboubi, M. Uhlemann, J. Amblard, Analysis of the magnetic force effect on paramagnetic species. J. Electroanal. Chem, 571 (2004) 85-91.

[29] V. Ganesh, D. Vijayaraghavan, V. Lakshminarayanan, Fine grain growth of nickel electrodeposit: effect of applied magnetic field during deposition, Appl. Surf. Sci, 240 (2005) 286-295. https://doi.org/10.1016/j.jelechem.2004.04.014.

[30] G. Ji, S. Tang, B. Xu, B. Gu, Y. Du, Synthesis of $CoFe_2O_4$ nanowire arrays by sol–gel template method. Chemical physics letters, Chem. Phys. Lett. 379 (2003) 484-489. https://doi.org/10.1016/j.cplett.2003.08.090.

[31] Y. Xu, D. S. Xue, D. Q. Gao, J. L. Fu, X. L. Fan, D.W. Guo, W. B. Sui, Ordered $CoFe_2O_4$ nanowire arrays with preferred crystal orientation and magnetic anisotropy, Electrochim. Acta. 54 (2009) 5684-5687. https://doi.org/10.1016/j.electacta.2009.05.012.

[32] J. J. Yuan, Q. Zhao, Y. S. Xu, Z. G. Liu, X. B. Du, G. H. Wen, Synthesis and magnetic properties of spinel $CoFe_2O_4$ nanowire arrays, J. Magn. Magn. Mater. 321 (2009) 2795-2798. https://doi.org/10.1016/j.jmmm.2009.04.036.

[33] S. R. Naik, A. V. SalKer, Change in the magnetostructural properties of rare earth doped cobalt ferrites relative to the magnetic anisotropy, J. Mater. Chem. 22 (2012) 2740–2750. https://doi.org/10.1039/C2JM15228B.

[34] I. C. Nlebedim, D. C. Jiles, Thermal effects on the magnetic properties of titanium modified cobalt ferrite, J. Appl. Phys. 117 (2015) 17A506. https://doi.org/10.1 063/1 .491 9229.

[35] R. H. Kodama, A. E. Berkowitz, Surface spin disorder in $NiFe_2O_4$ nanoparticles, Phys. Rev. Lett. 77 (1996) 394. https://doi.org/10.1103/PhysRevLett.77.394.

[36] L. Ajroudi, N. Mliki, L. Bessais, V. Madigou, S. Villain, C. Leroux, Magnetic, electric and thermal properties of cobalt ferrite nanoparticles, Mater. Res. Bull. 59 (2014) 49-58. https://doi.org/10.1016/j.materresbull.2014.06.029.

Figures captions

Figure. 1: SEM images of AAO membrane; cross sectional view (a,b) and plan view (c).

Figure. 2: Experimental setup of the electrodeposition process.

Figure. 3: J–V characteristic for the solution containing Co^{2+} and Fe^{2+} at 25 ^{o}C.

Figure. 4: Chronoamperograms of CoFe composite growth into AAO membranes at room temperature.

Figure.5: Growth of a layer on the nanowires surface after the total pores filling.

Figure. 6: XRD patterns of the synthesized $CoFe_2O_4$ nanowires: (a) annealed at 850 ^{o}C for 24 hours (b) electrodeposited in different nanoporous AAO membranes, (b) electrodeposited at various applied potentials, (d) magnetoelectrodeposited at various applied magnetic field, (e) field cooled at magnetic field of 0.6 T.

Figure. 7: Steps of samples preparation for SEM analysis.

Figure. 8: SEM images of $CoFe_2O_4$ nanowires electrodeposited into various nanoporous AAO membranes: top and cross sectional views for 20 nm (a, d), 100 nm (b, e), and 200 nm (c, f).

Figure.9: Hysteresis cycles recorded at 300 K for $CoFe_2O_4$ nanowires with different diameters.

Figure. 10: CA curves of electrochemical reduction of CoFe composite into 20 nm-AAO membranes at different applied potentials of -1 V, -1.1 V and -1.2 V.

Figure. 11: SEM images of $CoFe_2O_4$ nanowires electrodeposited at various potentials: (a) -1V, b) -1.1 V, and c) -1.2 V.

Figure. 12: 3D AFM micrographs of electrodeposited $CoFe_2O_4$ nanowires at -1 V (a), -1.1 V (b) and -1.2 V (c).

Figure. 13: Hysteresis loops of $CoFe_2O_4$ nanowire arrays grown at different deposition potentials. The $\parallel$ and $\perp$ signs indicate the sweeping magnetic field direction parallel and perpendicular to the substrate surface, respectively, during the SQUID-VSM measurement.

Figure. 14: CA curves of CoFe composite reduction in AAO membranes under different applied magnetic fields.

Figure. 15: MHD effect in electrodeposition under vertical applied magnetic field B.

Figure. 16: SEM images of the magneto-electrodeposited $CoFe_2O_4$ nanowires.

Figure. 17: AFM 2D surface topography of the magneto-electrodeposited $CoFe_2O_4$ nanowires: (a) B=0.4 T, b) B=0.5 T and (c) B=0.6 T.

Figure. 18: Hysteresis loops of the electrochemically deposited $CoFe_2O_4$ nanowires at various applied magnetic fields.
Figure. 19: Hysteresis loops of the annealed $CoFe_2O_4$ nanowires at 600 ^oC and 700 ^oC.
Figure. 20: Field cooling treatment of filled AAO membrane by $CoFe_2O_4$ crystallites.
Figure. 21: SEM images of field cooled $CoFe_2O_4$ nanowires. (a) partial dissolution, (b) total dissolution.
Figure. 22: Hysteresis loops of field cooled $CoFe_2O_4$ nanowires at 0.6 T.

Tables captions

Table. 1: Elemental composition of $CoFe_2O_4$ nanowires after the dissolution in 0.1 M NaOH.

Table. 2: Squareness ratios and coercive fields for $CoFe_2O_4$ nanowires.

Table. 3: *Calculated cell parameters and crystallite sizes.*

Table. 4: Elemental composition of the nanowires electrochemically grown at different applied potentials.

Table. 5: *Squareness ratios and coercive fields for $CoFe_2O_4$ nanowires.*

Table.6: EDS measurement for the magnetoelectrodeposited nanowires.

Table.7: Measured magnetic properties of $CoFe_2O_4$ nanowires grown by magneto electrodeposition in AAO templates

Table. 8: *Measured magnetic properties of the annealed $CoFe_2O_4$ nanowires*

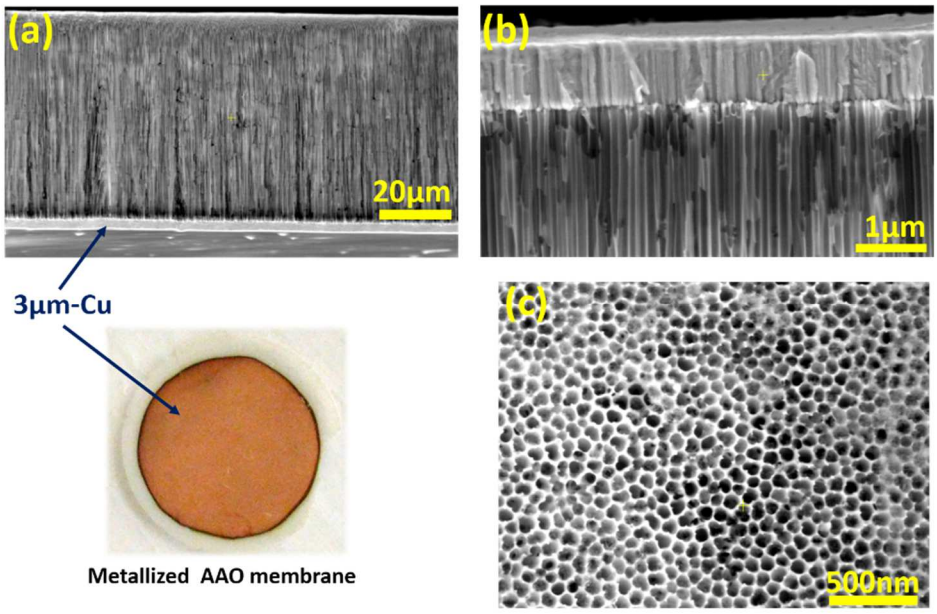

(a)
20µm
(b)
1µm
3µm-Cu
Metallized AAO membrane
(c)
500nm

Fig. 1

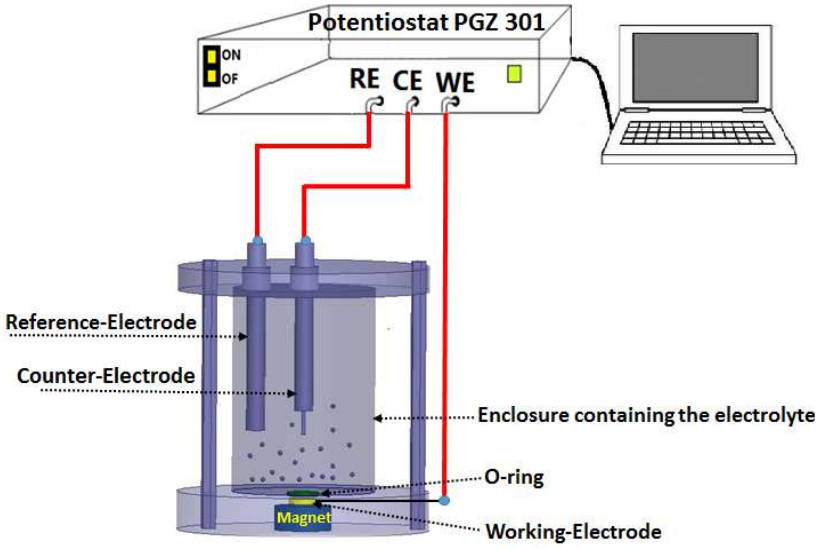

Potentiostat PGZ 301
ON
OF
RE CE WE
Reference-Electrode
Counter-Electrode
Enclosure containing the electrolyte
O-ring
Magnet
Working-Electrode

Fig. 2

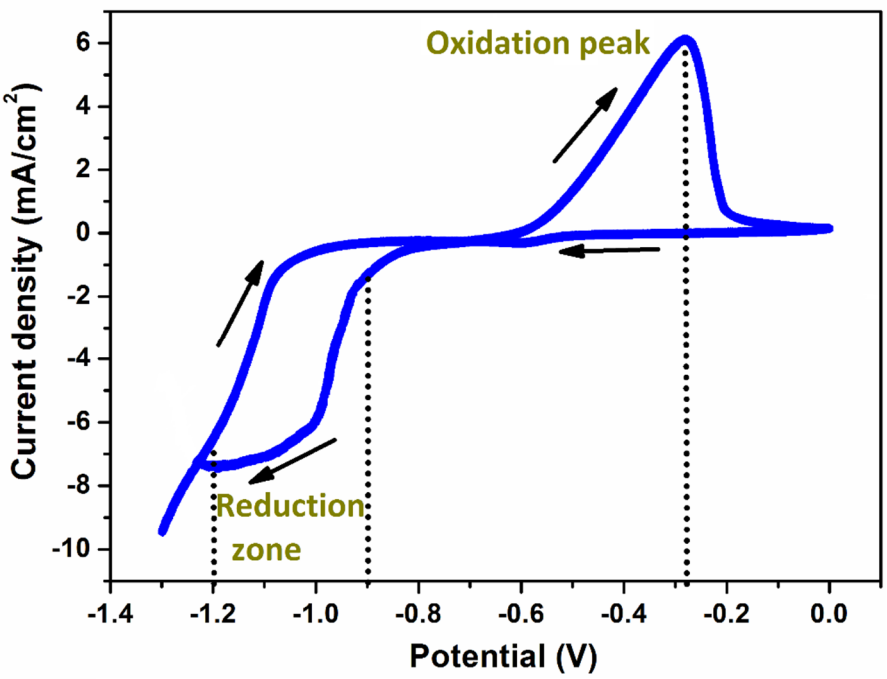

Oxidation peak
Reduction zone
Current density (mA/cm^2)
Potential (V)
6
4
2
0
-2
-4
-6
-8
-10
-1.4
-1.2
-1.0
-0.8
-0.6
-0.4
-0.2
0.0

Fig. 3

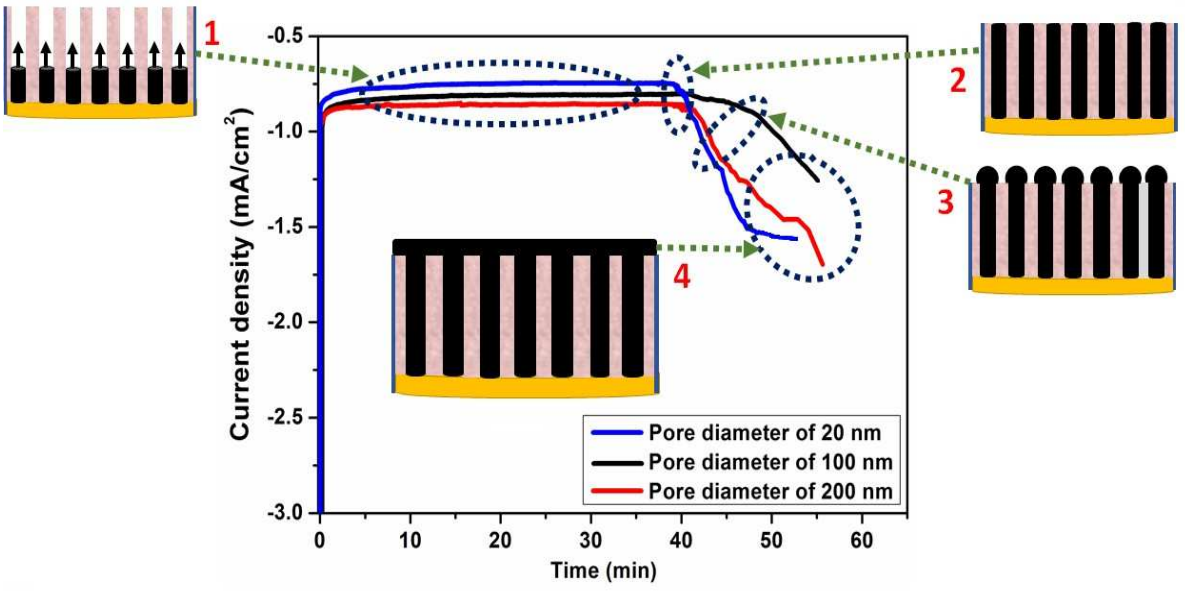

1
2
3
4
Current density (mA/cm^2)
Time (min)
Pore diameter of 20 nm
Pore diameter of 100 nm
Pore diameter of 200 nm
-0.5
-1.0
-1.5
-2.0
-2.5
-3.0
0
10
20
30
40
50
60

Fig. 4

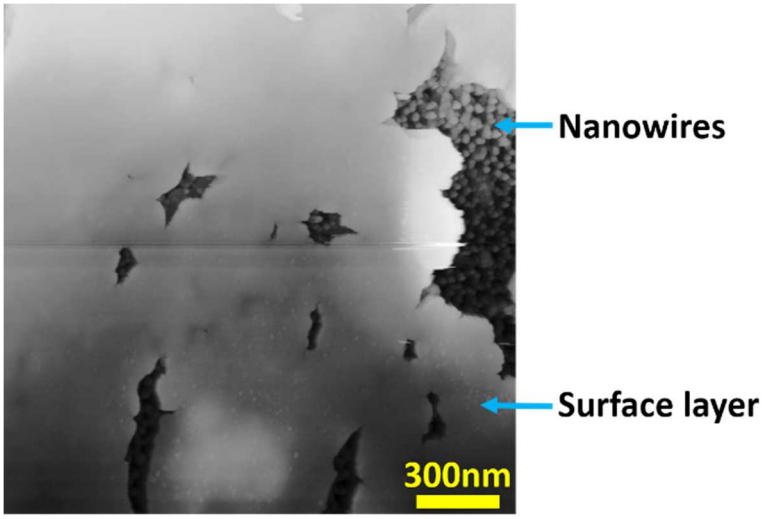


Fig. 5

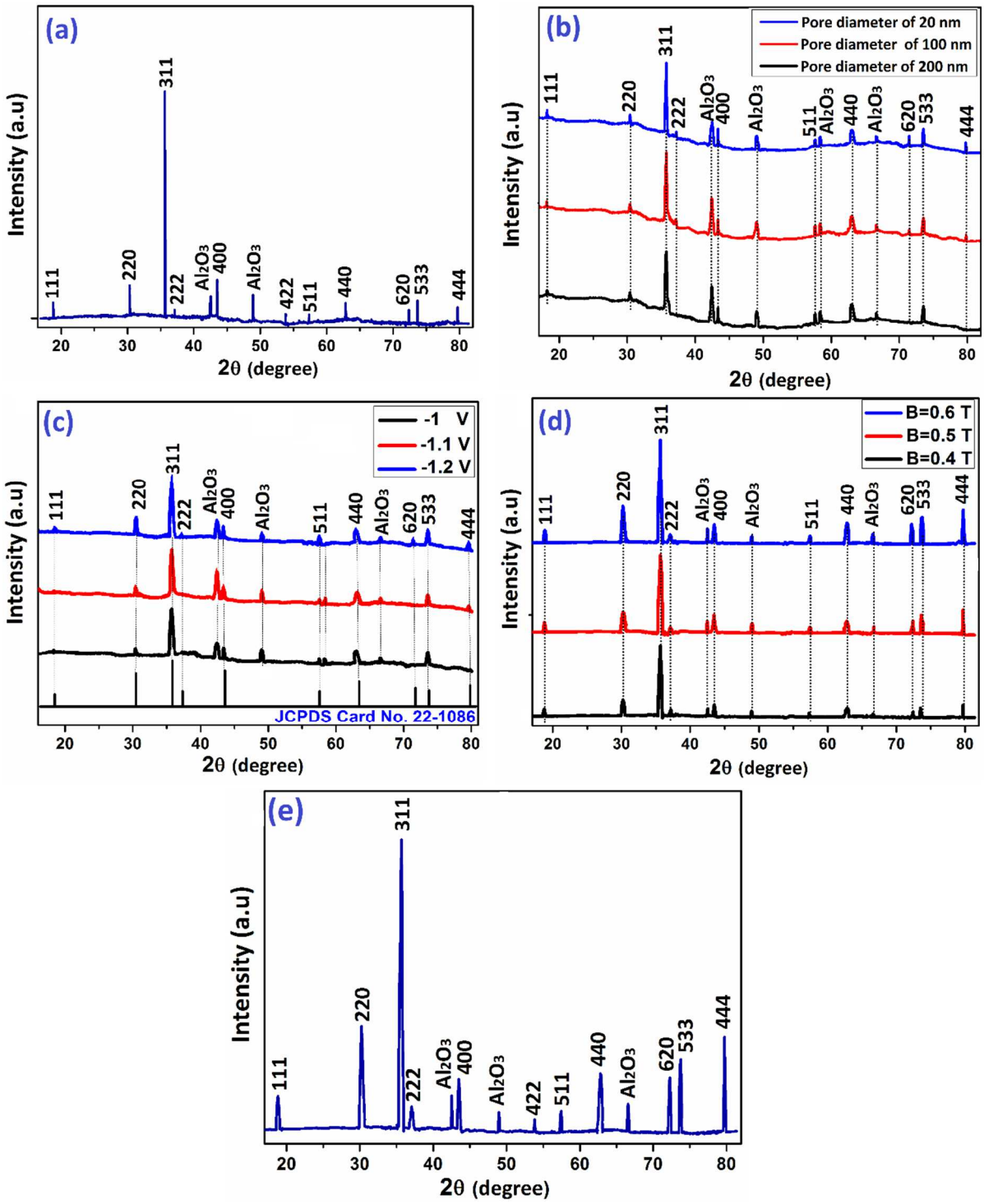

(a)
Intensity (a.u)
2θ (degree)
111
220
311
222
Al2O3
400
Al2O3
422
511
440
620
533
444
(b)
Pore diameter of 20 nm
Pore diameter of 100 nm
Pore diameter of 200 nm
(c)
-1 V
-1.1 V
-1.2 V
JCPDS Card No. 22-1086
(d)
B=0.6 T
B=0.5 T
B=0.4 T
(e)

Fig. 6

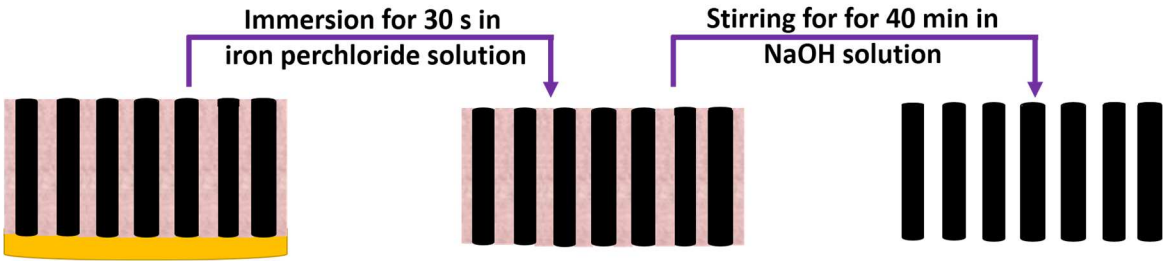

Immersion for 30 s in
iron perchloride solution
Stirring for for 40 min in
NaOH solution

Fig. 7

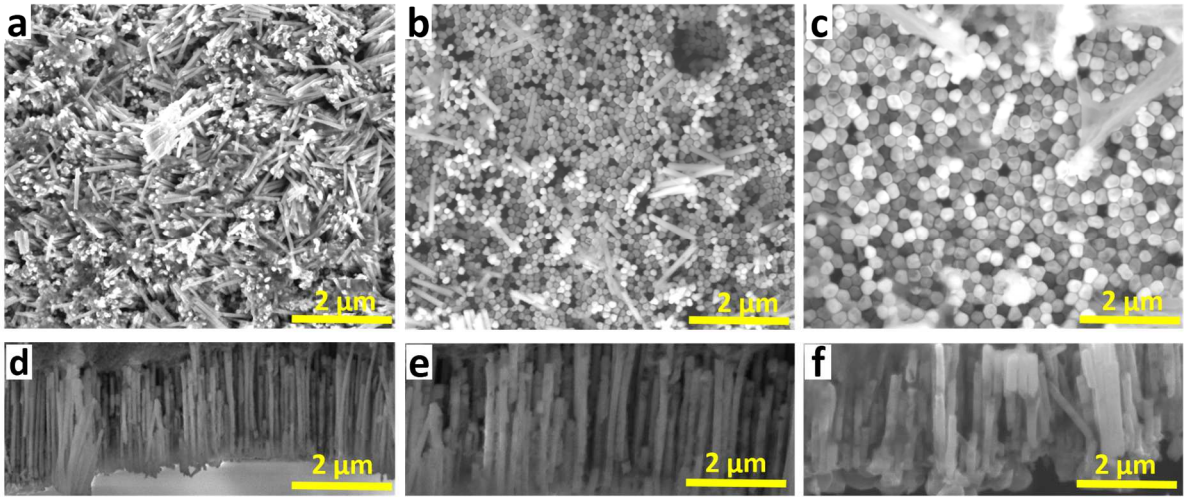

a
2 µm
b
2 µm
c
2 µm
d
2 µm
e
2 µm
f
2 µm

Fig. 8

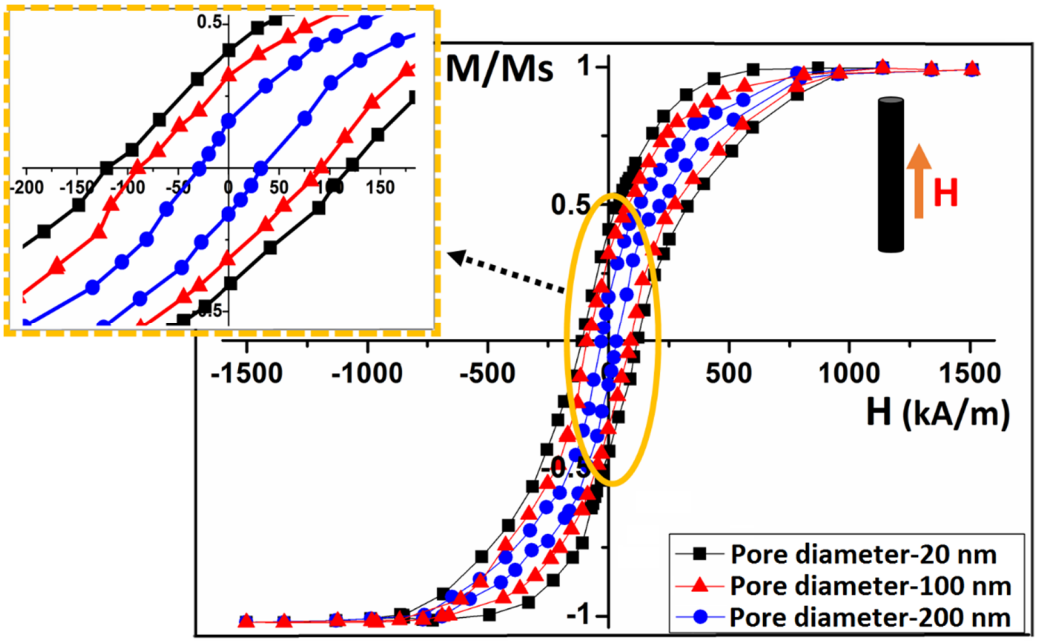

M/Ms
H
H (kA/m)
Pore diameter-20 nm
Pore diameter-100 nm
Pore diameter-200 nm

Fig. 9

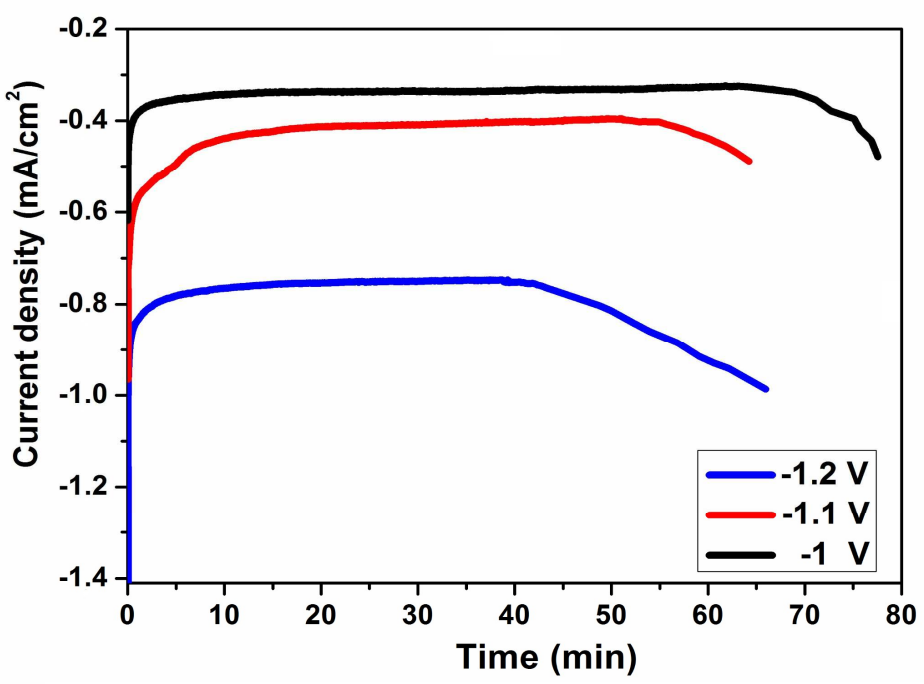

Current density (mA/cm²)
Time (min)
-1.2 V
-1.1 V
-1 V

Fig. 10

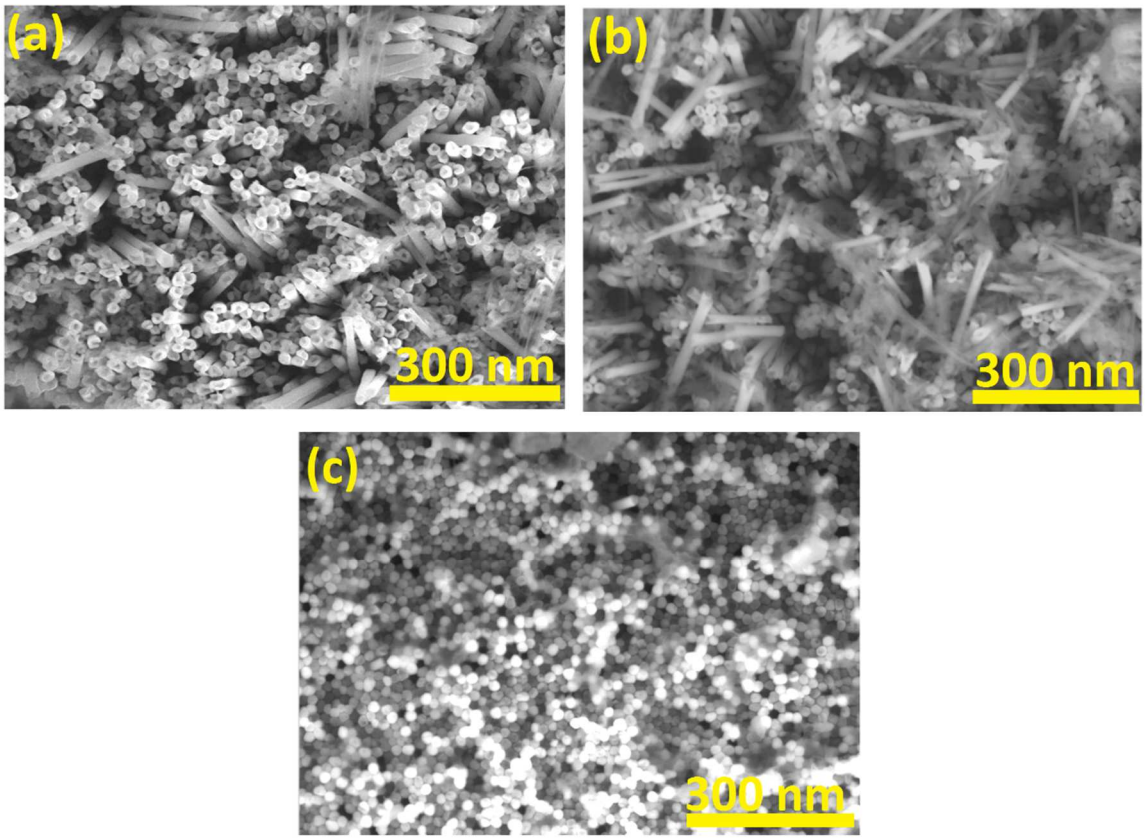


Fig. 11

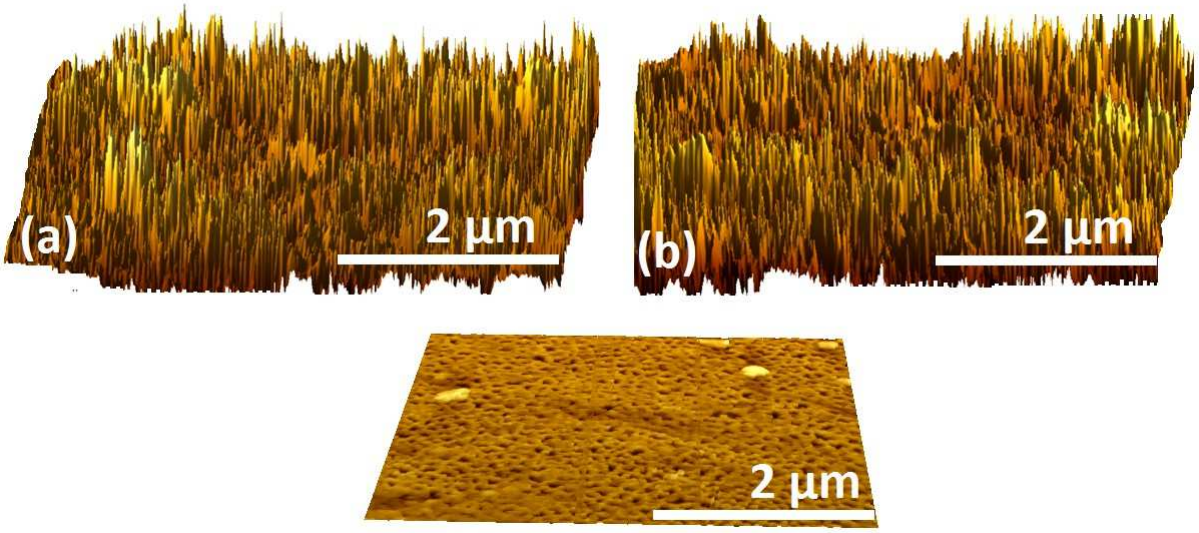


Fig. 12

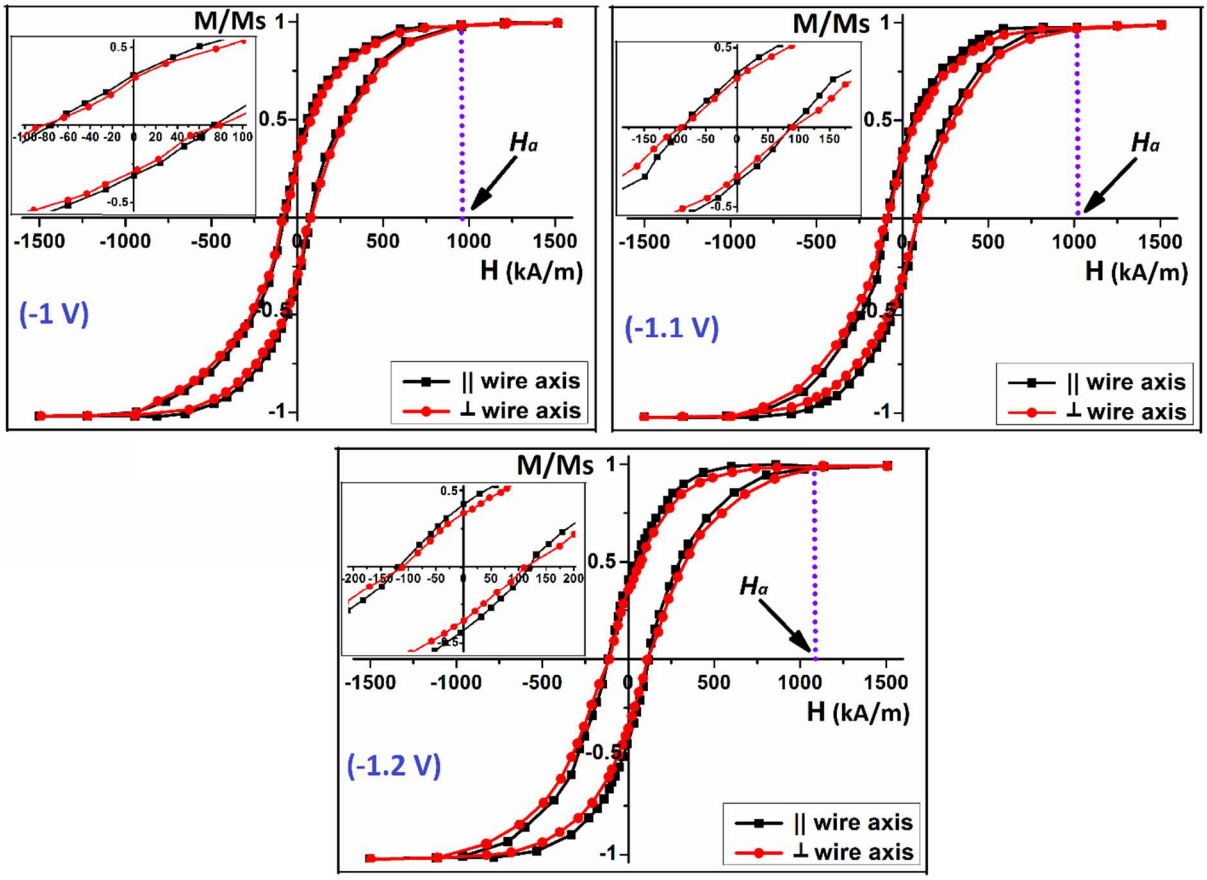


Fig. 13

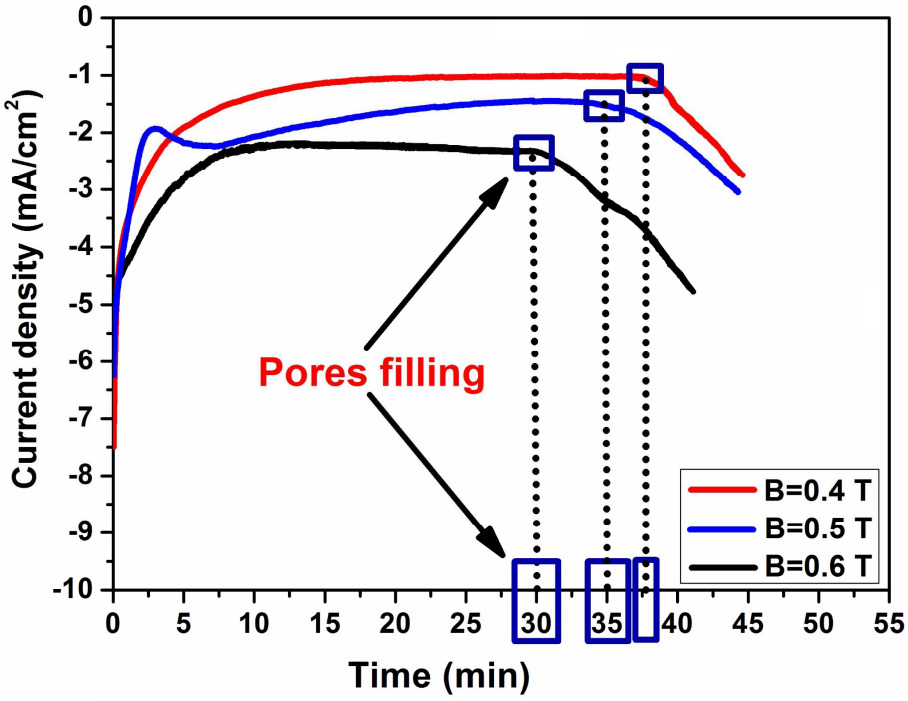

Current density (mA/cm^2)
Time (min)
Pores filling
B=0.4 T
B=0.5 T
B=0.6 T

Fig. 14

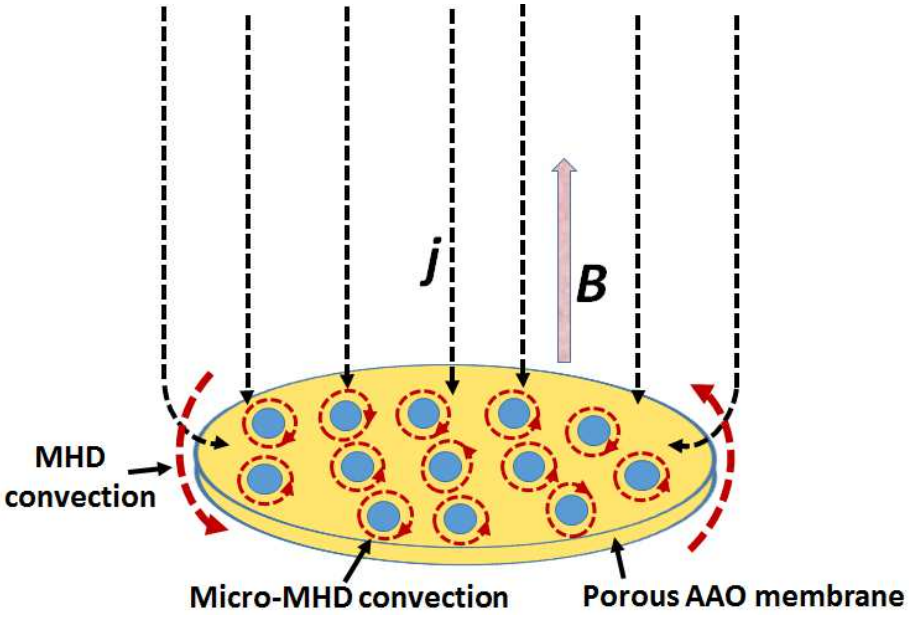

j
B
MHD convection
Micro-MHD convection
Porous AAO membrane

Fig. 15

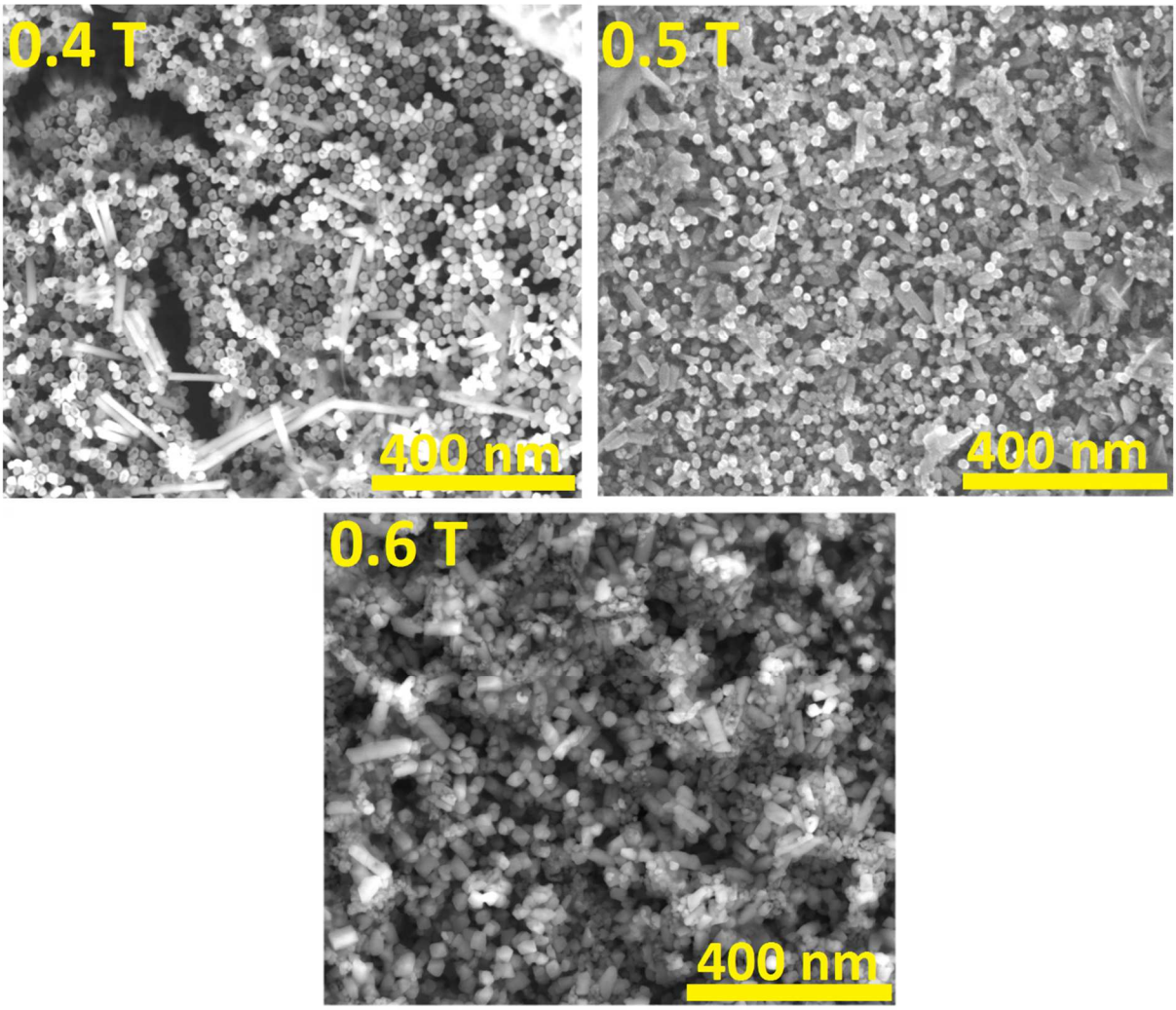


Fig. 16

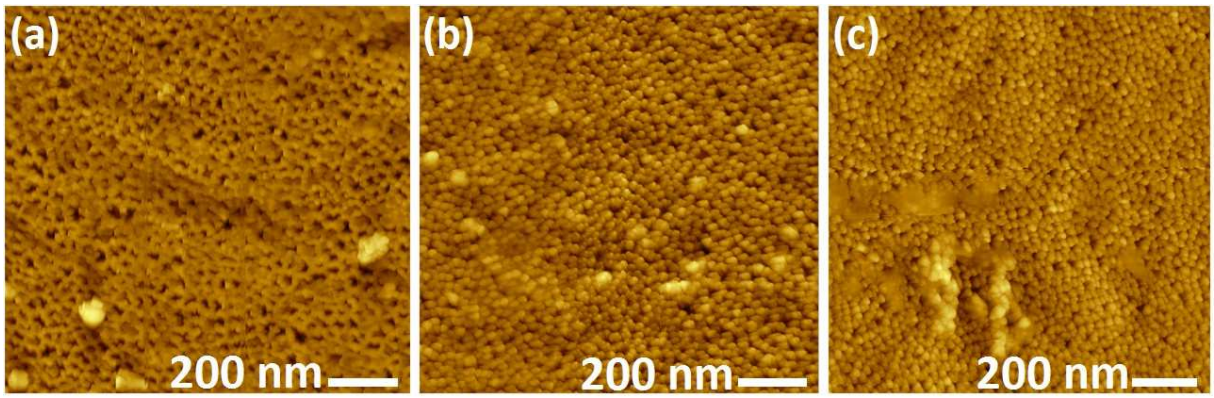


Fig. 17

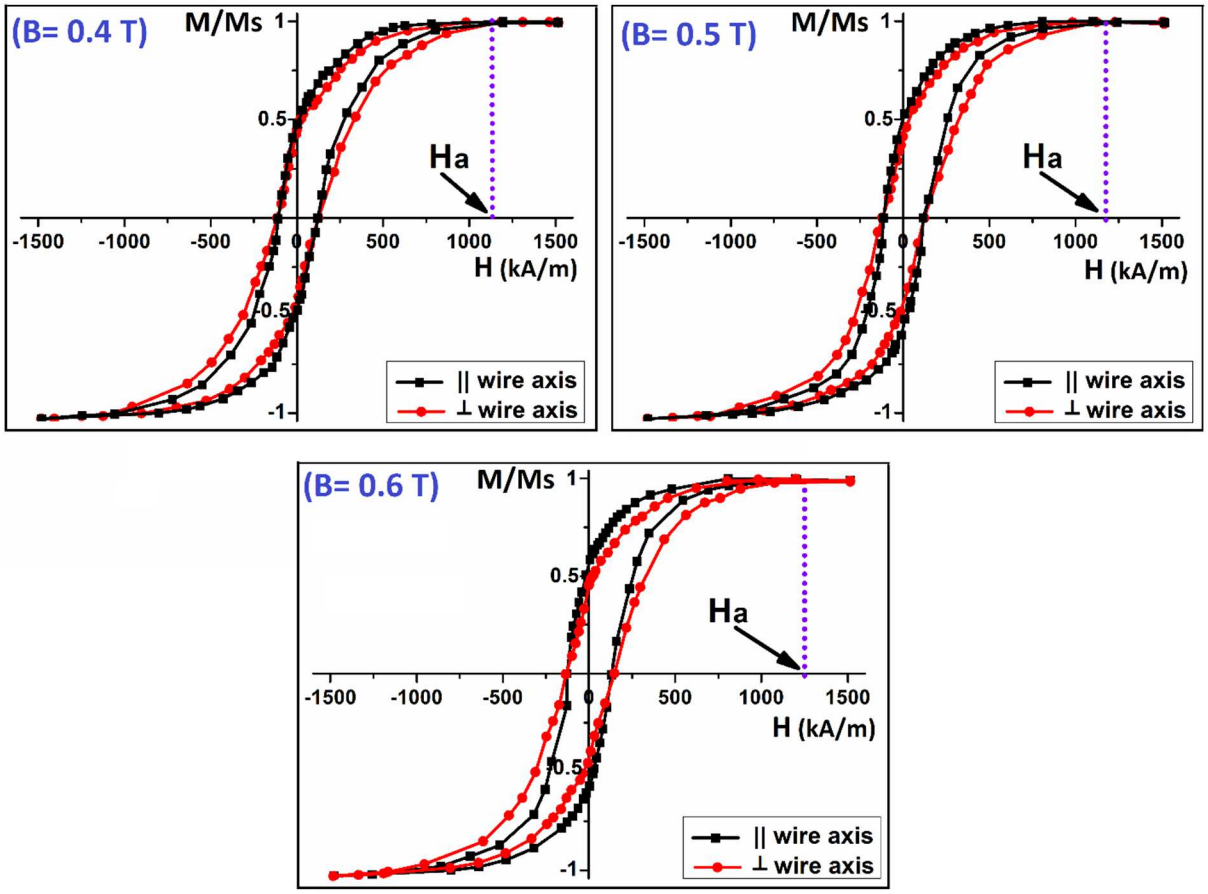

(B= 0.4 T)
M/Ms
Ha
H (kA/m)
|| wire axis
⊥ wire axis
(B= 0.5 T)
M/Ms
Ha
H (kA/m)
|| wire axis
⊥ wire axis
(B= 0.6 T)
M/Ms
Ha
H (kA/m)
|| wire axis
⊥ wire axis

Fig. 18

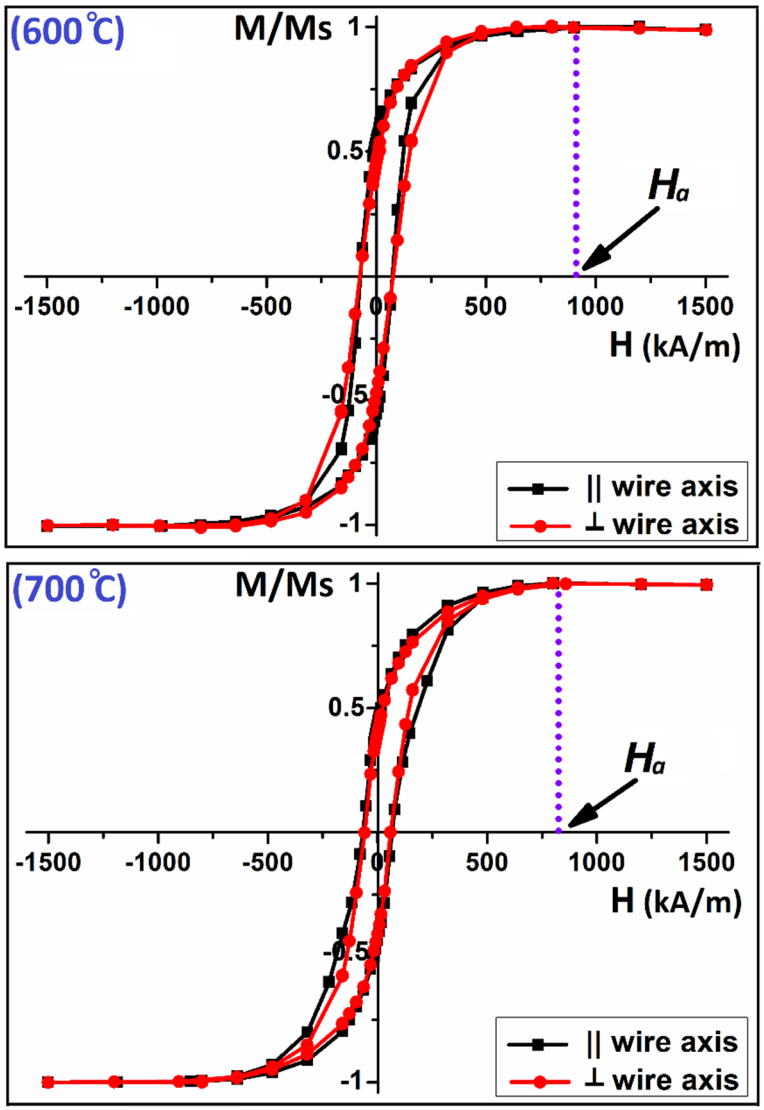

(600℃)
M/Ms
1
0.5
-0.5
-1
-1500
-1000
-500
0
500
1000
1500
H (kA/m)
H_a
|| wire axis
⊥ wire axis
(700℃)
M/Ms
1
0.5
-0.5
-1
-1500
-1000
-500
0
500
1000
1500
H (kA/m)
H_a
|| wire axis
⊥ wire axis

Fig. 19

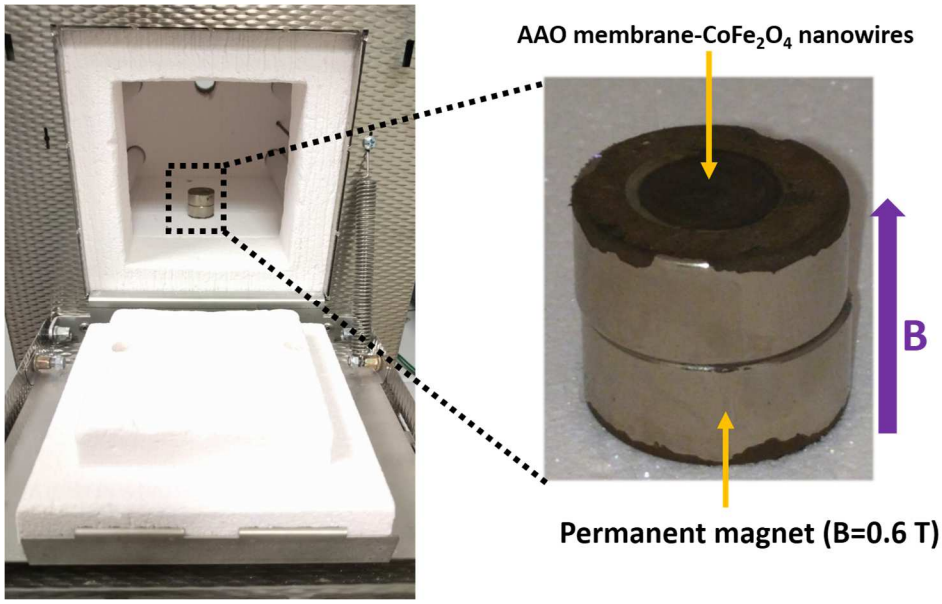

AAO membrane-$CoFe_2O_4$ nanowires
B
Permanent magnet (B=0.6 T)

Fig. 20

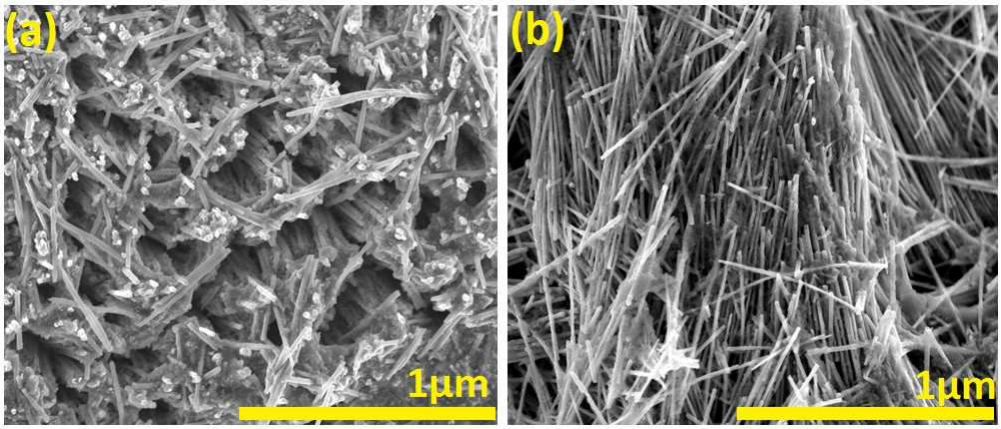

(a)
1μm
(b)
1μm

Fig. 21

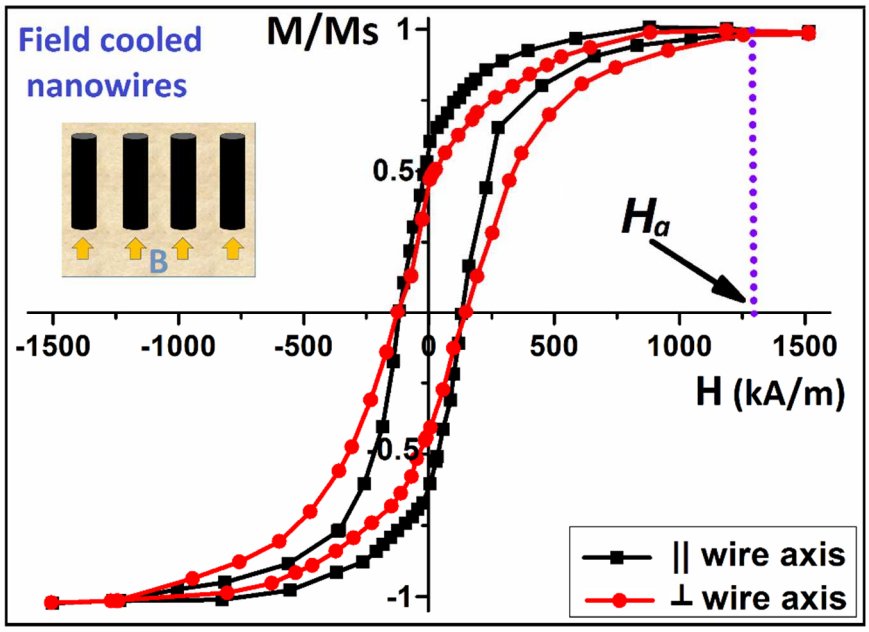

Field cooled
nanowires
B
M/Ms
1
0.5
-0.5
-1
-1500
-1000
-500
0
500
1000
1500
H (kA/m)
H_a
|| wire axis
⊥ wire axis

Fig. 22

	Pore diameter		
	200 nm	**100 nm**	**20 nm**
Elements		**At.%**	
$\mathbf{O-K}$	*60.05*	*62.25*	*58.08*
$\mathbf{Fe-K}$	*24.31*	*22.72*	*26.41*
$\boldsymbol{Co-K}$	*13.63*	*12.81*	*14.2*
$\mathbf{Al-K}$	*2.01*	*2.22*	*1.31*

Table. 1

	200 nm	**100 nm**	**20 nm**
$\boldsymbol{M_r/M_s}$	*0.16*	*0.32*	*0.4*
$\boldsymbol{H_c\ (kA/m)}$	*32*	*96*	*110*

Table. 2

Applied potential (V)	**Cell parameter (Å)**	**Crystallite size (nm)**
-1	8.325	15.17
-1.1	8.331	14.76
-1.2	8.354	14.04

Table. 3

	Applied potential		
	-1 V	**-1.1 V**	**-1.2 V**
Elements		**At.%**	
$\mathbf{O-K}$	*38.56*	*41.27*	*57.92*
$\mathbf{Fe-K}$	*33.05*	*34.18*	*25.81*
$\boldsymbol{Co-K}$	*28.39*	*24.55*	*16.44*

Table. 4

	Applied potential		
	-1 V	**-1.1 V**	**-1.2 V**
M_r/M_s (||)	*0.32*	*0.34*	*0.41*
$H_c\ (kA/m)$ (||)	*73*	*86*	*118*
M_r/M_s (⊥)	*0.30*	*0.31*	*0.36*
$H_c\ (kA/m)$ (⊥)	*79*	*90*	*111*
$\mu_o H_a$ (T)	*1.12*	*1.25*	*1.4*

Table. 5

	Applied magnetic field B		
	0.4 T	**0.5 T**	**0.6 T**
Elements		**At.%**	
O − K	*59.59*	*58.12*	*56.31*
Fe − K	*26.16*	*27.04*	*28.54*
Co − K	*14.25*	*14.84*	*15.15*

Table. 6

	B=0.4 T	**B=0.5 T**	**B=0.6 T**
M_r/M_s (||)	*0.47*	*0.5*	*0.55*
$H_c\ (kA/m)$ (||)	*120*	*116*	*131*
M_r/M_s (⊥)	*0.42*	*0.44*	*0.46*
$H_c\ (kA/m)$ (⊥)	*121*	*125*	*140*
$\mu_o H_a$ (T)	*1.42*	*1.44*	*1.5*

Table. 7

	600 °C	**700 °C**
$\boldsymbol{M_r/M_s}$ (||)	*0.52*	*0.43*
$\boldsymbol{H_c\,(kA/m)}$ (||)	*73*	*60*
$\boldsymbol{M_r/M_s}$ (⊥)	*0.46*	*0.41*
$\boldsymbol{H_c\,(kA/m)}$ (⊥)	*76*	*61*
$\boldsymbol{\mu_o H_a}$ (T)	*1.12*	*1.06*

Table. 8